



TÉCNICO
LISBOA

Kinetic modelling of biomass torrefaction as a pre-treatment for gasification

Bruno Filipe Bandarra Campos

Thesis to obtain the Master of Science Degree in

Mechanical Engineering

Supervisors : Prof. Miguel Abreu de Almeida Mendes
Dr. Raquel Inês Segurado Correia Lopes da Silva

Examination Committee

Chairperson: Prof. José Manuel da Silva Chaves Ribeiro Pereira
Supervisor: Dr. Raquel Inês Segurado Correia Lopes da Silva
Member of the Committee: Dr. Ana Filipa da Silva Ferreira

December 2021

Acknowledgments

Agradeço ao Professor Miguel Abreu de Almeida Mendes, a Doutora Raquel Inês Segurado Correia Lopes da Silva e a Ana Isabel Marques Ferreiro, pelo apoio e orientação prestados durante o decorrer da tese e pelo entusiasmo e empenho demonstrados com relação ao trabalho desenvolvido.

Um agradecimento especial a Ana Isabel Marques Ferreiro por toda a dedicação, preocupação e disponibilidade, pelas críticas sinceras e pela amizade, Obrigado por tudo Isabel!

Resumo

A biomassa apresenta alguns obstáculos à sua utilização, tais como a presença de humidade, baixa densidade volúmica, baixo poder calorífico, a presença de voláteis, e a sua natureza fibrosa podem levantar obstáculos para armazenar, transportar e converter a biomassa de forma eficiente em outros produtos de maior valor energético. A torrefação tem o potencial de melhorar essas propriedades, atuando como um pré-tratamento realizado a temperaturas entre os 200 e os 300 ° C, em atmosfera inerte, o que induz a decomposição parcial dos constituintes orgânicos da biomassa. Estudos experimentais desenvolvidos anteriormente mostram que a torrefação reduz a humidade na biomassa, confere hidrofobicidade, densificação energética, estabilidade bioquímica e facilidade de moagem. A modelação de um mecanismo cinético é essencial para definir o progresso das reações de modo a prever o perfil de gases e produtos libertados e quais as substâncias que os compõem. Com isto em vista, o trabalho desenvolvido adapta o comportamento do mecanismo cinético de torrefação. Estas adaptações consistem no ajuste de dois parâmetros, na retificação da cinética e coeficientes de algumas espécies, de forma a aproximar-se dos resultados experimentais para uma amostra de casca de noz, proveniente de resíduos agrícolas. Foram comparados com os resultados experimentais a quantidade de produtos e a composição dos gases libertados. O modelo cinético implementado, apesar de um erro relativo de 30 %, é o que apresenta a melhor previsão quando comparado com os restantes mecanismos cinéticos. O mecanismo, adaptado, resultou numa melhoria de 20 % quando comparado com o mecanismo antes de ser adaptado.

Palavras-chave: Biomassa, Torrefação, Modelação de mecanismo cinético

Abstract

Biomass presents some obstacles regarding its usage, such as the moisture content, low bulk density, low calorific value, high volatile and oxygen contents, and its tenacious and fibrous nature can create challenges to store, transport and efficiently convert biomass into fuels and other products. Torrefaction has the potential to improve biomass properties acting as a mild heat treatment in the temperature range of 200-300 °C under inert atmosphere inducing partial decomposition of the organic biomass components. The literature, focused on experimental studies, shows that torrefaction reduces the moisture content, confers hydrophobicity, biochemical stability, higher energy density and high grindability of biomass. It is well known that the kinetic modeling of biomass torrefaction is essential to define the progress of the decomposition-reaction paths and to evaluate the dependence of the rate of progression on process parameters, especially in regards to kinetic mechanisms that are able to predict release rate profiles, product yields and the product speciation, focused on the torrefaction uses. Therefore, the developed works consists of adapting a torrefaction kinetic scheme. These adaptations consist on adjusting two tunable parameters, correction of kinetic parameters and molar coefficients of specific species, in order to provide better results for a sample of nut shell, resultant from agricultural residues. It was compared against experimental data the product yields and gas composition. The implemented model, despite having a relative error of 30 %, it is the one with better predictions. The kinetic model, after the adaptations, presented an improvement of 20 % against the pre-modified kinetic scheme.

Keywords: Biomass, Torrefaction, Kinetic modelling

Contents

Acknowledgments	iii
Resumo	v
Abstract	vii
List of Tables	xi
List of Figures	xiii
Nomenclature	xv
1 Introduction	1
1.1 Motivation	1
1.2 Previous Studies	2
1.3 Objectives	6
1.4 Thesis Outline	7
2 Theoretical Foundation	9
2.1 Biomass composition	9
2.2 Thermogravimetric Analysis	11
2.3 Thermochemical processes	12
2.3.1 Pyrolysis	12
2.3.2 Torrefaction	13
3 Numerical Model	15
3.1 Model Structure	15
3.1.1 Initialise Variables and Reactor Initiation	16
3.1.2 ODE Solver	16
3.1.3 Values of interest	17
3.2 Model Assumptions	20
3.3 Kinetic scheme	21
4 Model adaptations and Results	25
4.1 Model Adaptations	27
4.2 Kinetic schemes comparison	32
4.3 Parametric Study	35

5 Conclusions **43**
 5.1 Future Work 43
Bibliography **45**

List of Tables

1.1	Experimental data from Strandberg et al. [4] for wood components in raw biomass and tor- rified, expressed on dry basis, where e.g. 260/8 stands for Temperature [° C]/ Residence time [minutes].	4
1.2	Experimental data from Strandberg et al. [4] for raw biomass and torrefied products, ex- pressed on dry basis, where e.g. 260/8 stands for Temperature [° C]/ Residence time [minutes].	5
3.1	kinetic scheme from Anca-Couce et al. [18], where y_{13} is defined by Eq. 3.16.	22
4.1	Biomass composition in wt. % from nut shell sample.	25
4.2	Biomass proximate and ultimate analysis, in wt. % dry from nut shell sample.	26
4.3	Deviations from sensibility test to y_{13}	29
4.4	kinetic scheme adaptation.	32
4.5	Deviations from the experimental results.	34

List of Figures

1.1	Energy balance from APREN [1].	2
1.2	Biomass torrefaction severity in regard to the temperature; raw biomass, mildly torrefied biomass, medium torrefied biomass and severe torrefied biomass.	3
2.1	Primary components chemical composition adapted from [21], where (a) is Cellulose, (b) Hemicellulose and (c) Lignin.	10
2.2	Thermogravimetric analysis of hemicellulose, cellulose and lignin, from [26].	12
2.3	Stages of torrefaction and propriety changes of biomass during the process, adapted from [28].	14
3.1	Flowchart showing the structure of the implemented model and how the different parts are interconnected.	16
3.2	Pyrolysis kinetic scheme from Ranzi et al. [34].	21
4.1	Used temperature profiles on experimental setup to obtain TGA (TGA Profile) and the profile of the released gases (Reactor Profile).	27
4.2	Value of y_{13} as a function of temperature (a) and reaction rate of reaction 13 from kinetic scheme presented on Table 3.1 as a function of the temperature (b).	28
4.3	Influence of y_{13} on the product yields at $300\text{ }^{\circ}\text{C}$ (a) and gas composition at $300\text{ }^{\circ}\text{C}$ (b).	28
4.4	Relative error as a function of x_i and HCE1, where cells 1 to 5 represents the smallest errors in increasing order.	29
4.5	Relative error of gas yield (a) and liquid yield (b) as a function of x_i and HCE1.	30
4.6	Relative error of CO yield (a) and CO ₂ yield (b) as a function of x_i and HCE1.	30
4.7	Contributions of reactions to the total release rate of CO (a) and CO ₂ (b).	32
4.8	Mass yield profile (a) and respective rate (TGA) (b).	33
4.9	Release rates of CO (a) and CO ₂ (b).	33
4.10	Product yields (a) and gas composition (b).	34
4.11	Mass evolution of the mass yield as a function of the temperature and residence time for the adapted model (a) and pyrolysis (b).	36
4.12	Liquid yield as a function of the temperature and residence time for the adapted model (a) and pyrolysis (b).	37

4.13 Liquid yield as a function of the temperature and residence time for the adapted model (a) and pyrolysis (b).	38
4.14 LHV as a function of the temperature and residence time for the adapted model (a) and pyrolysis (b).	39
4.15 Energy densification as a function of the temperature and residence time for the adapted model (a) and pyrolysis (b).	40
4.16 Gas LHV as a function of the temperature and residence time for the adapted model (a) and pyrolysis (b).	41
4.17 Liquid LHV as a function of the temperature and residence time for the adapted model (a) and pyrolysis (b).	42

Nomenclature

Symbols	Explanation	Unit
AA	Acetic Acid	-
E	Activation energy	J mol^{-1}
Al	Aluminium	-
Ca	Calcium	-
C	Carbon	-
CO_2	Carbon dioxide	-
CO	Carbon monoxide	-
Cl	Chlorine	-
ρ	Density	Kg m^{-3}
E_ρ	Energy density	-
η_E	Energy yield	-
h	Enthalpy	KJ Kg^{-1}
HCE1	Hemicellulose depolymerization reaction	-
HCE2	Hemicellulose ring opening reaction	-
HHV	Higher heating value	MJ Kg^{-1}
H	Hydrogen	-
R	Ideal gas constant	$\text{J mol}^{-1} \text{K}^{-1}$
Fe	Iron	-
h_g	Latent heat of steam	KJ Kg^{-1}
LHV	Lower heating value	MJ Kg^{-1}
Mg	Magnesium	-
Mn	Manganese	-
m	Mass	Kg
H/C	Mass coefficient ratio of Hydrogen content and Carbon content	-
O/C	Mass coefficient ratio of Oxygen content and Carbon content	-
Y	Mass fraction	-
\dot{m}	Mass rate	Kg s^{-1}

η_m	Mass yield	-
CH ₄	Methane	-
<i>M</i>	Moisture	%
M_w	Molecular weight	Kg Kmol ⁻¹
$\dot{\omega}$	Net production rate	Kmol m ⁻³ s ⁻¹
N	Nitrogen	-
<i>n</i>	Number of moles	-
O	Oxygen	-
<i>P</i>	Parameter	-
P	Phosphorus	-
K	Potassium	-
<i>A</i>	Pre-exponential factor	s ⁻¹
$k(T)$	Reaction rate	s ⁻¹
Si	Silicon	-
Na	Sodium	-
S	Sulfur	-
TANN	Taxifolin	-
<i>T</i>	Temperature	K
Ti	Titanium	-
TGL	Triglyceroid	-
ω	Weight	-
wt.%	Weight percentage	-
<i>Yield</i>	Yield	%

Subscripts

exp	Experimental
g	Gas
gen	Generated
0	Initial
i	Iterable
liq	Liquid
num	Numerical
p	Particle
P	Products
R	Reactants
sp	Specie
tor	Torrified

Chapter 1

Introduction

1.1 Motivation

For the past few years, fossil fuels have been the main energy source to meet the energy demands across the globe, even though its availability is limited and the use of fossil fuels has proven to cause a negative impact on the environment, such as the greenhouse effect, among others. As a consequence, renewable energy sources have been rising to eventually replace fossil fuels. However, the current renewable energy sources have to be strategically placed accordingly to the geographic profile of a given region, besides its dependency on weather conditions, which causes intermittency on its availability. The unreliability of renewable energies is seen as a major disadvantage compared to fossil fuels, which are available regardless of the weather. In this regard, biomass has a great advantage over other renewables, such as solar, hydropower or windpower, since it can be stored and transported, allowing it to be used where and when necessary, regardless of the weather conditions and the geographic profile of the location. Some biomass types may only be available during a given season, therefore the biomass at use might have to be adjusted to respect the seasonality of biomass.

Currently, the energy demand in Portugal is met mostly by importation, with renewable energies as a major asset that is produced nationally. Renewable energies contribution have been increasing over the past few years, between January and June of 2021, with renewables corresponding to 70% of the total energy produced, whereas only 30% coming from the non-renewable sources, according to Associação Portuguesa de Energias Renováveis (APREN) [1].

Hydropower and wind power have the largest contribution to the renewable energy balance (35.8% and 26% respectively). Bioenergy appears on third place accounting for around 6,5%, as it can be perceived in figure 1.1.

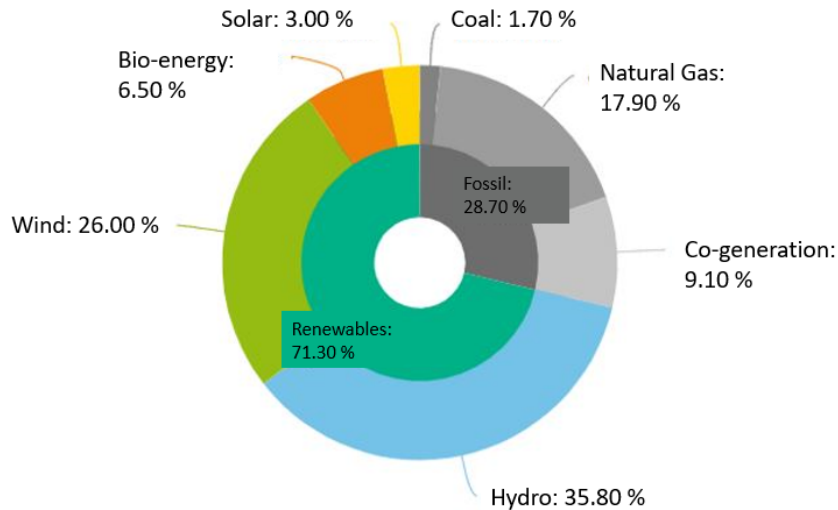


Figure 1.1: Energy balance from APREN [1].

Portugal, according to Ferreira et al. [2], has shown a great potential for biomass use in energy production, with an estimated potential of 42489.7 GW h Year⁻¹. However, this potential is currently unachievable due to the usage of biomass in other industries, such as paper and furniture. There are residues resultant from some activities which might be used in bioenergy production, such as agricultural residues, but these usually present 35% lower energy density when compared to coal. The difference between the energy content constitutes a challenge, which delays biomass use in the energy market. In order to overcome this obstacle, biomass can undergo thermochemical processes to improve its thermodynamic properties, increasing its calorific value, therefore becoming a more competitive fuel.

Gasification, pyrolysis and torrefaction are some examples of the available thermochemical processes. Torrefaction in particular, is a biomass pre-treatment, run under low temperatures, under inert atmosphere [3–6], which causes the partial decomposition of biomass, uniforming its properties to be used in other thermochemical processes. Torrefaction also improves biomass capacity to be stored and transported [3], since the resultant biomass becomes hydrophobic and less voluminous as some of the mass is lost due to light devolatilization. Currently, woody biomass are the most utilized on thermochemical conversion processes, even though residues from agricultural activity have no competition by other industries, making it a high availability biomass source. The agricultural residues can bring even more challenges due to the higher variability within the residues. In this context, there is a necessity to better predict the behaviour of this biomass type under the torrefaction processes to spread its use in the bioenergy industry.

1.2 Previous Studies

Torrefaction has several parameters which can be optimised as a function of the desired outcome. The temperature at which torrefaction undergoes is one of the most important aspects of the pre-treatment. The suitable temperature ranges are dependent on the biomass application, as, in general,

higher temperatures provide a lower energy yield and mass. Some studies suggest temperature ranges between 200 and 300 °C [3, 6–8]. However, Wei-Hsin Chen et al. [9] suggests that torrefaction below 240 °C results in light torrefaction severity which has a low impact in biomass properties, since the higher the severity the more notorious are the changes in biomass properties [10]. Figure 1.2 presents a visual representation of the different torrefaction severities, from raw, to mildly torrefied, medium torrefied and severe torrefied biomass.

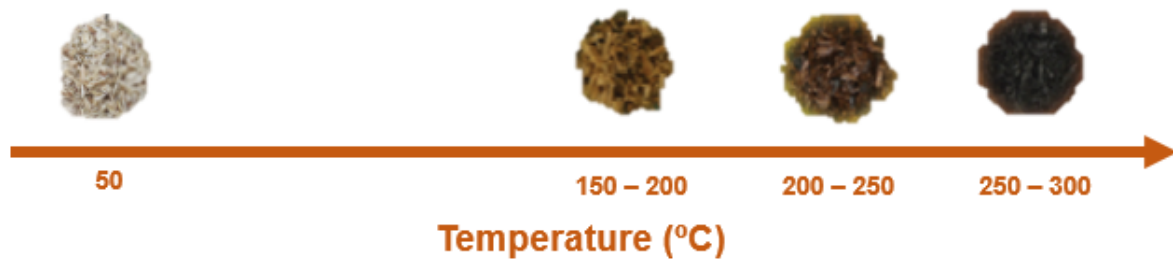


Figure 1.2: Biomass torrefaction severity in regard to the temperature; raw biomass, mildly torrefied biomass, medium torrefied biomass and severe torrefied biomass.

Strandberg et al. [4] studied the effects of temperature and residence time on torrefaction of spruce wood. It was found that the total content of hemicelluloses for a residence time of 8 minutes had a reduction of 12% at 260 °C and 80% at 310 °C. Cellulose, on the other hand, for the same residence time of 8 minutes, showed a less severe reduction. At 310 °C, the reduction was only about 14% but an increase in the residence time to 25 minutes caused total degradation of the cellulose content. This effect demonstrates the predominance of temperature over residence time and the dependency of both parameters on each other. Another guideline for the optimal temperature corresponds to the desired yields. Wannapeera et al. [10] indicates that the solid yield decreases with temperature and/or residence time, whereas liquid and gas yields increase for the same conditions. The desired products dictate which temperature is the most suitable to perform torrefaction. Depending on the desired final products, higher temperatures can be used, since the biggest mass loss occurs in the 250 - 350 °C range [10, 11], which is also the range suggested by Ke-Miao Lu et al. [5] as a more suitable range for torrefaction. Usually, torrefaction aims to thermal degrade hemicellulose (Table 1.1), hence high temperatures promote too much devolatilization of this particular component. An extensive decrease in volatile matter is not desirable, since the solid phase loses too much chemical energy to the gas phase [6, 8]. According to Basu [8] and Strandberg et al. [4], the highest temperature for torrefaction would be 300 °C, since temperatures above 300 °C promote excessive devolatilization. From Table 1.1 it can be seen that hemicellulose is the most affected component under torrefaction conditions. Moreover, the predominance of temperature over residence time can also be verified.

Table 1.1: Experimental data from Strandberg et al. [4] for wood components in raw biomass and torrefied, expressed on dry basis, where e.g. 260/8 stands for Temperature [$^{\circ}$ C]/ Residence time [minutes].

	Lignin(%)	Cellulose(%)	Hemicellulose(%)	Extractives(%)
Raw	30.9	41.7	26.0	1.4
260/8	31.3	43.5	23.9	1.3
260/25	37.9	44.9	15.1	2.1
285/16.5	44.0	46.2	7.2	2.6
310/8	45.0	46.9	5.5	2.6
310/25	94.7	1.9	0.1	3.3

As mentioned before, temperature has been shown to have a dominant effect over residence time, although these proprieties are not interchangeable [4, 8] and residence time should be determined based on the chosen temperature. The typical residence time is between a few minutes and 1 hour, with Wanapeera et al. [10] indicating that residence times should not be longer than the 2 hours, since after 1h the effect on mass loss diminishes [8, 10]. Bergman et al. [6] suggests residence times of 5 to 15 minutes are often sufficient to most applications. Nonetheless, residence time can be adjusted depending on the desired torrefaction severity and set temperature. High temperatures need less residence time than lower temperatures do in order to achieve the same torrefaction severity. Longer residence time promotes more thermal conversion, since it destroys the least reactive components of hemicellulose and causes bigger losses in volatile matter, increasing torrefaction severity [11]. It is also worthy of note that the maximum achievable severity is determined by the temperature and not by the residence time. As an example, torrefaction bellow 240° C, regardless of increasing the residence time will always results in light torrefaction severity [9].

The longer residence time of torrefaction, when compared to other thremochemical processes, is more forgiving on the particle size that can be torrefied, since a longer residence time allows the particle to reach the desired temperature with ease. Bergman et al. [6] suggests that woodchips with 2 cm thickness can still be torrefied without heat transfer limitations, whereas, for example, for pyrolysis a finer particle is required. On the other hand, the pre-treatment causes partial degradation of biomass, which improves the grindability of biomass, with a maximum reduction of 95% in the energy required in the grinding process [4] (as it can be seen on Table 1.2), which is supported by other studies as Tumurulu et al. [3] and Repellin et al. [12]. The reduction in milling energy showed a linear correlation with the hemicellulose reduction, whereas cellulose and lignin showed no similar correlation [4]. This transformation is crucial to save energy in milling biomass to be used on other thermochemical processes which require a finer particle size.

Regarding the inert conditions at which torrefaction takes place, usually it is run under an inert atmosphere [6]. Ke-Miao Lu et al. [5] tested torrefaction under an inert (N_2) atmosphere and torrefaction under air atmosphere. It was concluded that an atmosphere with air resulted in lower solid yield and lower heating values when compared to inert atmosphere and, as a consequence, it is not recommended. For temperatures between 250 and 350° C the difference in solid yield ranged from 9.4% to 33.1% (where the N_2 had higher solid yields) and a difference between 0.2 and 9.0 MJ/Kg, where the

difference grows along with the temperature increment [5].

As it was mentioned on the previous topic, torrefaction adds value to biomass as a fuel, this is due to the changes that occur in the hydrophobicity and heating values of biomass. Strandberg et al. [4] suggests that moisture content in torrefied biomass can decrease by 50% or more, when compared to raw biomass, varying accordingly to the severity achieved throughout torrefaction (Tumurulu et al. [3] and Bergman et al. [6] also noted this effect). The hydrophobicity can be explained since raw biomass has hydroxyl (OH) groups on its composition. These groups form hydrogen bonds with water molecules, which allows moisture to attach to biomass [8]. During torrefaction the hydroxyl groups are destroyed, forming nonpolar unsaturated structures, which causes hydrophobicity on biomass [3, 13].

The heating value quantifies the amount of energy per unit of mass of a given substance. Throughout torrefaction, the energy and mass yield, which are strongly dependent on temperature [6], are affected. As it has been mentioned before, torrefaction leads to devolatilization, which implies the loss of low energy molecules to the gas phase and, therefore, a loss in mass and energy. Since the mass yield decreases more than the energy yield [6, 13], the energy available per unit of mass is greater than before. This process is known as energy densification and it occurs as a consequence of the solid residue becoming richer in carbon (where both H/C and O/C ratios decrease), which causes an increment in carbon content and higher heating values [4–6, 14] as it is presented on Table 1.2. The energy densification typically varies from 1.00 to 1.20 [14]. The reported transformation helps to shorten the gap between biomass and fossil fuels, as a fuel with more energy per unit of mass is usually more attractive to the industry.

Table 1.2: Experimental data from Strandberg et al. [4] for raw biomass and torrefied products, expressed on dry basis, where e.g. 260/8 stands for Temperature [° C]/ Residence time [minutes].

	HHV (MJ/Kg)	H(%)	C(%)	O(%)	Milling energy consumption [KWh/ton]
Raw	20.37	5.9	50.4	43.6	123 ± 17
260/8	20.65	5.9	51.4	42.3	69 ± 14
260/25	21.51	5.9	53.6	40.0	51 ± 3.3
285/16.5	22.23	5.7	55.2	38.6	29 ± 2.6
310/8	22.42	5.8	55.8	37.9	25 ± 1.4
310/25	27.78	5.0	69.2	25.0	8.9 ± 0.5

Currently, most applications of torrefied biomass are in electric power plants, in co-firing processes combined with coal [3]. Due to the propriety changes that occur, torrefied biomass can serve other bioenergy applications, such as gasification or even an alternative over wood pellets due to its hydrophobic nature. Some companies have used light torrefaction as a treatment for wood, to improve isolation and to take advantage of the hydrophobic nature of torrefied biomass for example.

From the previous analysis, torrefaction is a multiple parameter process where it is difficult to be aware of all the changes biomass undergoes, which raises the necessity to predict biomass behaviour. The experimental setups required to assure optimal operating conditions can be challenging, therefore a numerical model able to predict biomass devolatilization is necessary. Most of available models are

currently for pyrolysis, which do not predict accurately the behaviour under torrefaction conditions.

A study by Sarvaramini et al. [15], stemming from a pyrolysis kinetic scheme, could provide optimal kinetic parameters, where the results could fit the experimental volatile release for mild and severe torrefaction. Despite the model predictions fitting the experimental data, the results are valid for woody biomass and do not account for the different hemicellulose types, which highly varies on agricultural biomass. Another downside is that the model uses lumped reactions for the components which might disregard the interactions of the gas phase. Other study by Mehrabian et al. [16] tried to adapt a kinetic scheme from Ranzi et al. [17] as an attempt to identify and quantify the gas products accurately. The adapted model provided good predictions for hardwood biomass. However, the same was not verified for softwood biomass due to the lack of distinction between hemicellulose types. The model could predict qualitatively the gas yields but not quantitatively. There was a strong under prediction of water and acetic acid as well. Nonetheless, the same kinetic scheme was adapted with further modifications by Anca-Couce et al.[18].

The adaptations of the Ranzi et al. [17] kinetic scheme by Anca-Couce et al. [18] were able to predict the mass loss evolution and product yields with the presence of secondary reactions. These changes allowed a more accurate prediction of the generated products but still does not account for the different hemicellulose types, which leads to inaccuracies on non-woody biomass. A study by Debiagi et al. [19] introduced the variability of the different hemicellulose types by adjusting two molar coefficients and its ratios, which will be explained further in Chapter 4.

From the gathered information, it is difficult to predict the devolatilization that occurs during torrefaction. The present work uses torrefaction as a pre-treatment for gasification of agricultural residues biomass, therefore it is extremely important to predict accurately the devolatilization of biomass, in order to predict which torrefaction setup provides the best compromise between the acquired proprieties of torrefied biomass and volatile matter preservation.

1.3 Objectives

The general objective of the present work is to study the kinetic scheme of torrefaction as a pre-treatment for gasification of agricultural residues, more specifically:

- Implementation of an existing kinetic scheme for torrefaction, able to be used on gasification pre-treatment.
- Adaptation of the existing kinetic scheme.
- Comparison between the adapted model and experimental data.

The developed work contributes to fill in a gap on the kinetic modelling research of non-woody biomass for torrefaction conditions.

1.4 Thesis Outline

This thesis is structured as follows: Chapter 1 presents the motivation and relevance to develop the present work, along with previous studies concerning biomass torrefaction, which is the subject of study. Following Chapter 1, is Chapter 2 which provides theoretical background regarding biomass composition and thermochemical conversion methods to better understand the work that follows. Chapter 3 describes the numerical model in use, followed by the provided results in Chapter 4. Lastly, Chapter 5 covers the main conclusions of the developed work and some aspect which can be further explored, presented as future work.

Chapter 2

Theoretical Foundation

According to the United Nations Framework Convention on Climate Change (UNFCCC, 2005) biomass is defined as “*non-fossilized and biodegradable organic material originating from plants, animals and micro-organisms*” [13].

2.1 Biomass composition

There is a large variety of biodegradable organic material across the globe. Therefore, biomass is organized in specific groups, based on origin and/or composition. Vassilev et al. [20] suggests the following classification categories:

- Wood and woody biomass;
- Herbaceous and agricultural biomass;
- Aquatic biomass, animal and human biomass wastes;
- Contaminated biomass and industrial biomass wastes (semi-biomass);
- Biomass mixtures.

Within the mentioned classifications above, there is still a great diversity, this is due to the high variability in biomass composition as it depends on genetics and growth environment [20]. The properties of the soil, weather conditions, fertilizers and pesticides contribute further for diversity, causing a great impact on the final composition of biomass. In regards to the elemental composition of biomass, Vassilev et al. [20] states the elements in its decreasing order of abundance: C, O, H, N, Ca, K, Si, Mg, Al, S, Fe, P, Cl, Na, Mn and Ti. However the mineral content of biomass is highly correlated to the properties of the soil and pesticide usage.

Biomass is structured by the cell walls, which are the primary components [13], extractives and ash. Extractives are organic and inorganic components which do not take part in the integral structure of biomass, such as saccharides, carbohydrates, proteins, oils, aromatics, lipids, phenols, waxes, resins, organic acids, among others. The aforementioned compounds can be extracted using water, ethanol,

benzene and toluene based solvents [20] and present higher mean concentrations on herbaceous and agricultural biomass and lower for wood and woody biomass [20]. Ash designates the inorganic material found in biomass. This inorganic material is found in a smaller scale when compared to solid fossil fuels. The presence of inorganic material, as mentioned before, is highly variable across biomass types. In addition to this, specific parts of the plant might be more favorable to accumulate inorganic material. Wood barks have a higher propensity to accumulate inorganic material, as it usually has more impurities from the soil, whereas a wood stem has a lower tendency to accumulate soil impurities, resulting on a lower concentration of inorganic material [20]. Cell wall material corresponds to biomass structural components, which provide the structural support against mechanical stresses and strength for the plant [3, 20]. These structural components are cellulose, hemicellulose and lignin, which are represented in Figure 2.1.

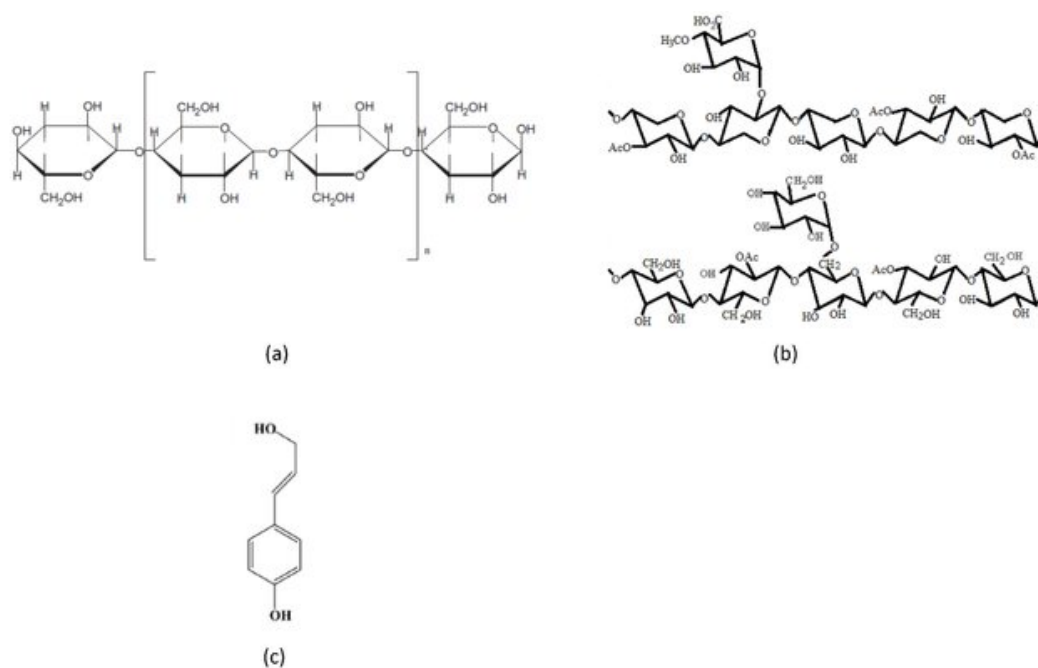


Figure 2.1: Primary components chemical composition adapted from [21], where (a) is Cellulose, (b) Hemicellulose and (c) Lignin.

Lignin is not only part of the primary and second cell wall components but it also acts as an embedding material for adjacent cells [13, 20]. It is a highly branched phenolic polymer [13] with an amorphous structure [20]. Lignin, out of the three main structural components is the one with the highest heat resistance and highest char formation [3]. Lignin is decomposed between 280 and 500 °C [3]. Cellulose ($C_6H_{10}O_5$) can be defined as a long-chain carbohydrate with a fibrous structure, which presents a crystalline structure made out of glucose molecules [13, 20]. Due to its crystalline structure, it is more resistant to thermal degradation when compared to hemicellulose. The decomposition reactions occur for temperatures between 240 - 350 °C [3]. Hemicellulose ($C_5H_8O_4$), in opposition to cellulose, has an amorphous structure and presents a highly branched chain structure [13, 20]. When exposed to heat hemicellulose decomposition reactions initiates at 150 °C and it increases significantly for temperatures

around 220-280 °C [3]. Generally, hemicellulose degradation emits light volatiles with low char production when compared with cellulose thermal degradation [3]. Due to its branched structure, hemicellulose may form another compounds, presenting therefore different behaviours under thermal degradation, mainly on the generated products. According to Zhou et al. [22], hemicellulose can be further divided into xylans, mannans, xyloglucan, galactans and β -glucan. The distinction of hemicellulose types can help to better predict the released volatile matter and being able to account for the diversity inherent to biomass.

Xylans are hemicellulose polysaccharides that commonly present in hardwood and herbaceous biomass. Xylans can classify as homoxylans and heteroxylans, depending on the presence or absence of certain functional groups on the side chains. Heteroxylans are composed by glucuronoxylans, arabinoxylans and arabinoglucuronoxylans or glucuronoarabinoxylans [22]. The major hemicellulose polysaccharide in hardwood, ranging from 15 to 30 % of dry weight, is glucuronoxylans [22, 23]. On the other hand, herbaceous biomass types are predominant in arabinoxylans [22]. Mannans, according to Zhou et al. [22], can be categorized into homomannans, galactomannans, glucomannans and galactoglucomannans. These components make 20-25% of softwood biomass weight. In contrast, mannans account for less than 5% in hardwood biomass with its contribution entirely due to glucomannans presence.

2.2 Thermogravimetric Analysis

Thermogravimetric analysis (TGA) is a testing method done on samples in order to determine weight changes on the tested material with respect to change in temperature [24]. The weight measurements along with time and temperature, allow to determine the rate of change in weight, which can be used to identify the main reactions involved and to estimate its kinetic parameters. Determining these parameters results in the prediction of the thermal behaviour of the sample. However, this process is limited due to the simultaneous of the reactions involved, although, torrefaction behaviour is considered to be the combination of each individual components [25], therefore, TGA is a powerful tool to determine stages and composition of multi-component systems. This can be seen in Figure 2.2, as the contributions of each individual component to the overall mass loss are represented. Figure 2.2 is representative of a TGA for pyrolysis, where it presents the mass percentage and mass loss rate as a function of the temperature. Moreover, TGA can also be useful to determine atmosphere effects, quantify moisture, ash and volatile content of the tested sample.

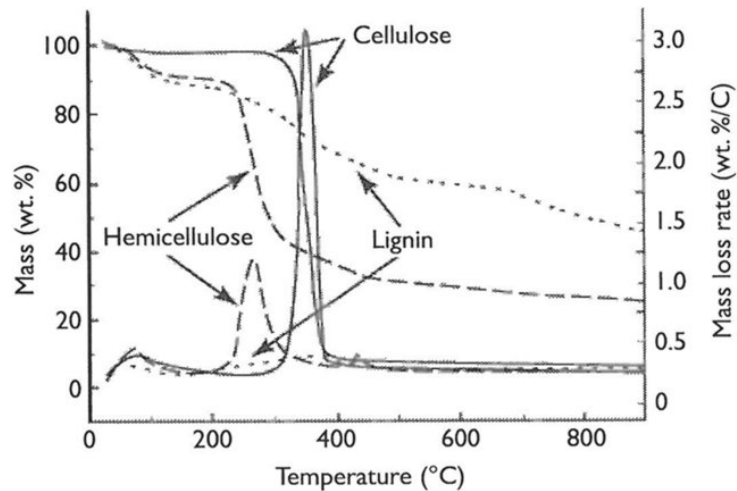


Figure 2.2: Thermogravimetric analysis of hemicellulose, cellulose and lignin, from [26].

2.3 Thermochemical processes

As mentioned before in section 1.1, raw biomass presents major inconveniences when compared to the practicality of fossil fuels. Biomass usually has low bulk density (overall space occupied by an amount of biomass material), low heating value and hydrophilic nature, which results in high moisture content [4]. The lower the heating value, the more biomass quantities are needed to output the same energy, which can be regarded as a disadvantage in terms of storage, transportation and feed handling for co-generation processes [3]. The lack of a constant particle size makes biomass less suitable for co-firing. The high moisture content increases transportation costs and provides a favorable environment for microorganisms (bacterial and fungal), which promotes biomass decomposition, reducing its quality. If moist, the efficiency in thermochemical processes is decreased [3], limiting biomass usage in energy applications. Having this in mind, biomass is treated via specific thermochemical processes in order to improve its properties [5] and/or usage. Thermochemical conversion can be achieved through combustion, torrefaction, pyrolysis, gasification and liquefaction [2, 8]. Due to the nature of the present work, only pyrolysis and torrefaction will be further explained.

2.3.1 Pyrolysis

Demirbas et al. [27] defines pyrolysis as the “*degradation of biomass by heat in the absence of oxygen, which results in the production of charcoal (solid), bio-oil (liquid) and fuel gas products*”. Pyrolysis can also be performed with a limited supply of oxidizing agents, which decreases gasification to a great extent [2]. Depending on particle size, temperature, heating rates and residence time, pyrolysis parameters can be changed to meet different final products. A slow heating rate, performed for a low final temperature and a long residence time promotes char production, whereas a high heating rate with a short residence time and a final temperature of 450-600 °C optimizes the liquid production. Gasification is promoted by a high final temperature, in the 700-900 °C range, long residence time and a slow

heating rate [2].

2.3.2 Torrefaction

Torrefaction is a biomass pre-treatment [3–6], that is run at low temperatures, under inert atmosphere, and with a heating rate lower than 50 °C/min [6]. Torrefaction resembles pyrolysis, the difference being the temperature range, in which lower heating rates are utilized. This serves the purpose of obtaining greater solid yields, with relatively small liquid and gas yields. Torrefaction targets, mainly, hemicellulose thermal degradation, although other components might still be affected. This partial decomposition leads to some devolatilization, resulting in loss of mass and chemical energy, where the mass loss is greater than the energy loss [6]. Therefore, the resultant solid has a greater energy content per unit of mass. This implies a higher heating value, which upgrades biomass thermal properties and its value as a fuel.

What occurs during torrefaction can be described based on the temperature regime biomass is subjected to and it is represented in Figure 2.3. Tumurulu et al. [3] (in accordance with Basu [8]) suggests four regimes as it follows:

Regime A - (50 - 120 ° C): This regime is called *Nonreactive drying* (or *Predrying* [28]). For this temperatures, there are no changes in the chemical composition. The main phenomenon is the loss in moisture content, which leads to reduced porosity and shrinkage of biomass.

Regime B (120 - 150 ° C): Lignin softens and serves as a binder.

Regime C (150 - 200 ° C): Regime known for *Reactive drying* (or *Postdrying* [28]). In contrast to regime A, the breakage of hydrogen and carbon bonds start to occur. This leads to the depolymerization of hemicellulose. At this point, the structural deformation is irreversible.

Regime D (200 - 300 ° C): *Destructive drying* where most reactions take place. This regime results in carbonization and devolatilization. For temperatures bellow 250 °C, the mass loss is at its minimum [3, 10], which is a reflex of limited hemicellulose decomposition. For temperatures above 250 °C, hemicellulose decomposes extensively. Lignin and cellulose show limited devolatilization and carbonization. At this point the cell is completely destroyed, therefore, biomass becomes brittle and nonfibrous.

The Figure 2.3 presented bellow, represents the above described stages, and provides a visual representation of the given stages and its propriety changes.

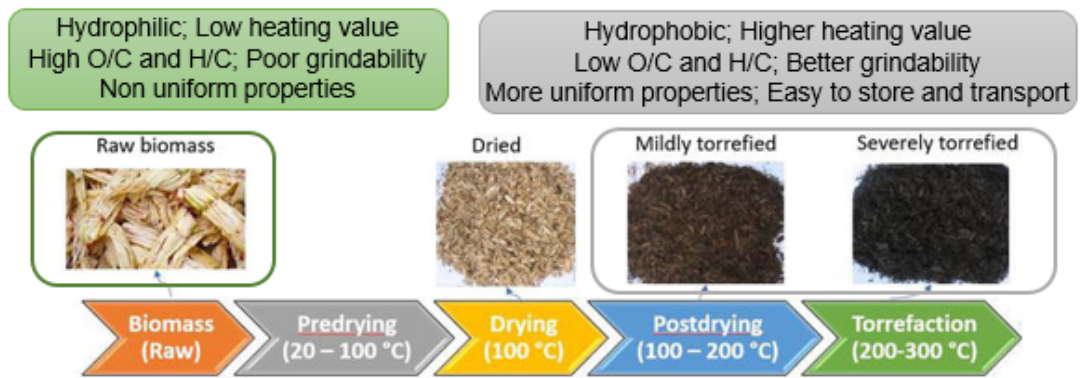


Figure 2.3: Stages of torrefaction and propriety changes of biomass during the process, adapted from [28].

Chapter 3

Numerical Model

The purpose of the present numerical model is the representation of a torrefaction kinetic scheme that predicts accurately the influence of torrefaction on biomass, from the behaviour of the particle to the products speciation. In order to solve the species conservation and the reaction rates throughout the process, a stiff ordinary differential equation solver was used (CVODE). The temperature profile, biomass composition, reactor, pressure, carrier gas are given as inputs to the model. The implementation relies on an adaptation of a previous numerical model developed by Anca-Couce et al. from [18]. The implementation is done in Python [29], utilizing Cantera [30] reaction kinetics library.

3.1 Model Structure

The general structure of the implemented model presented in this chapter may be described by a flowchart, which can be seen in Figure 3.1. It details the order in which the different parts of the implemented model are used and how they interconnect.

The implemented model starts by initialising all the variables, covering the imposed temperature profile, time step, biomass composition, pressure and carrier gas and other similar variables.

The following step is to update the temperature, for the imposed temperature profile, and update the forward reaction rates accordingly. Through the release rate adjustment, the mass conservation of biomass is calculated. The cycle repeats with similar time intervals, until the stop condition is reached, which is defined as the end of the imposed temperature profile. The results are stored and values of interest, such as yields, heating values, among others are calculated.

This whole procedure is, as mentioned shown in Figure 3.1.

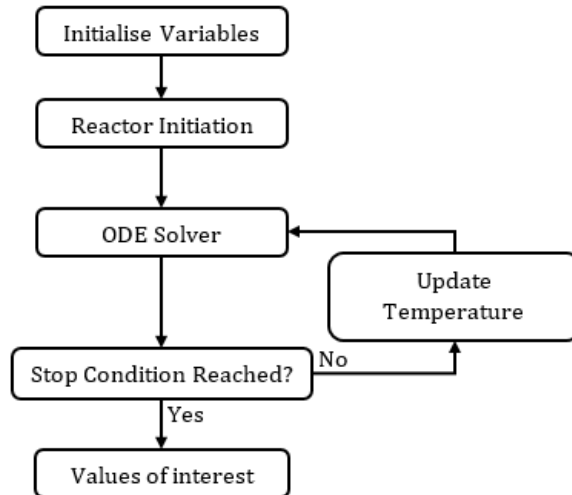


Figure 3.1: Flowchart showing the structure of the implemented model and how the different parts are interconnected.

3.1.1 Initialise Variables and Reactor Initiation

The initializing section of the implemented model purpose is to initialize major variables which are necessary to run the kinetics of the particle. Biomass composition, which is given as a model input, is accounted for in this stage. The reactor is initialized as a homogeneous closed system, with a fixed volume and adiabatic and chemically-inert walls. The initial mass fractions are set for each component along with pressure and temperature profile.

3.1.2 ODE Solver

The solver at hand aims to solve the species conservation and calculate the reaction rates, in order to do so, a stiff ordinary differential equation solver [31] in Python [29] was used. As the imposed temperature profile is updated the forward reaction rates are calculated, as those are temperature dependent. Due to the undergoing devolatilization, some species are lost from the solid phase to the gas phase, therefore, the fractions of species present in all phases are updated. The process is done until the stop condition is reached.

Governing Equations

The rate constant, $k(T)$, describes the relation between the molar concentration of the reactants and the rate of reaction. The rate constants are calculated by Arrhenius equation, which is described by the temperature, activation energy, E , and a pre-exponential factor, A . The activation energy, E , is the minimum energy required for the reaction to occur. The pre-exponential factor, A , is determined experimentally and represents an empirical correlation between the temperature and the reaction rate.

The rate constant is defined in Eq. 3.1, which is calculated similarly for all the reactions.

$$k_i(T) = A_i \cdot \exp\left(\frac{-E_i}{R \cdot T}\right) \quad (3.1)$$

Where:

A_i is the pre-exponential factor [s^{-1}].

E_i is the Activation energy [$J \text{ mol}^{-1}$].

R is the ideal gas constant of $8.3144 \text{ [J mol}^{-1} \text{ K}^{-1}]$

T is the temperature of the species within the reactor [K]

Mass conservation is described by the following equations based on Ferreiro et al. [31]:

$$m_p \frac{dY_{sp}}{dt} = \dot{m}_{sp, gen} \quad (3.2)$$

Where:

m_p is the mass of the particle [Kg]

Y_{sp} is the mass fraction of a given specie

$\dot{m}_{sp, gen}$ is the mass rate generated of a given specie [$Kg \text{ s}^{-1}$]

$$\dot{m}_{sp, gen} = \dot{\omega} \times \frac{M_{w, sp}}{\rho_g} \times m_{p, 0} \quad (3.3)$$

Where:

$M_{w, sp}$ is the molecular weight of a given specie [$Kg \text{ kmol}^{-1}$]

ρ_g is the density of the gas [$Kg \text{ m}^{-3}$]

$\dot{\omega}$ is the net production rate [$Kmol \text{ m}^{-3} \text{ s}^{-1}$]

$m_{p, 0}$ is the initial mass of the particle [Kg]

Total particle mass is given by:

$$m_p = m_{p, 0} \times \sum_{\text{solid, sp}} Y_{\text{solid, sp}} \quad (3.4)$$

3.1.3 Values of interest

This section of the implemented model calculates values of interest which allow for a better understanding and quantification of the occurring changes throughout torrefaction.

Yields

Product yields are given by Eq. 3.5.

$$Yield_i = \frac{\sum(M_{w, sp, i} \times Y_{sp, i})}{m_{p, 0}} \quad (3.5)$$

where:

$Yield_i$ is the yield of a product, with i being solid, liquid or gas [%]

$M_{w, sp, i}$ is the molecular weight of a given product yield specie [Kg kmol⁻¹]

$Y_{sp, i}$ is the mass fraction of a given product yield specie

Similarly, the yields of certain species within the given product yield is given by Eq. 3.6.

$$Yield_{sp, i} = \frac{\sum Y_{sp, i}}{Yield_i} \quad (3.6)$$

where:

$Yield_{sp, i}$ is the yield of a given product specie [%]

Energy densification

According to Pimchuai et al. [11] energy densification is given by Eq. 3.7.

$$E_\rho = \frac{\eta_E}{\eta_m} = \frac{HHV_{tor}}{HHV_{raw}} \quad (3.7)$$

Where:

E_ρ is the energy density

η_E is the energy yield [%]

η_m is the mass yield [%]

HHV_{tor} is the higher heating value of torrefied product [MJ Kg⁻¹]

HHV_{raw} is the higher heating value of raw product [MJ Kg⁻¹]

According to Strandberg et al. [4] mass and energy yield are described by Eq. 3.8 and Eq. 3.9 respectively.

$$\eta_m = \frac{m_{tor}}{m_{raw}} \quad (3.8)$$

Where:

m_{tor} is the mass of torrefied product [Kg]

m_{raw} is the mass of raw product [Kg]

$$\eta_E = \eta_m \frac{HHV_{tor}}{HHV_{raw}} \quad (3.9)$$

Heating values

Nhuchhen et al. [32] gathered from previous studies several correlations and verified with 26 biomass samples which correlations were the most accurate to measure the high heating value (HHV) of torrefied biomass. It was concluded that 3.10 presented the best outcome. Hence, this was the correlation used throughout the present work.

$$HHV = 32.7984 + 0.0053C^2 - 0.5321C - 2.8769H + 0.0608CH - 0.2401N \quad (3.10)$$

Where:

C is the mass fraction of carbon content.

H is the mass fraction of hydrogen content.

N is the mass fraction of nitrogen content

Eq. 3.11, from Basu [13] correlates the lower heating value (LHV) with the HHV, which can be used to determine the LHV of torrefied biomass.

$$LHV = HHV - h_g \left(\frac{9H}{100} - \frac{M}{100} \right) \quad (3.11)$$

where:

LHV is the lower heating value [MJ Kg^{-1}]

M is the moisture percentage [%]

h_g is the latent heat of steam, for 100°C , of $2260 \text{ [KJ Kg}^{-1}\text{]}$

In order to calculate the heating value of the liquid products, it is necessary to determine the heating value of each formed specie, which is given by Eq.3.12.

$$LHV_{sp} = \frac{h_{RP, sp}}{M_{sp}} \quad (3.12)$$

where:

$h_{RP, sp}$ is the enthalpy of combustion of a given specie [KJ Kg^{-1}]

This enthalpy of combustion is defined as the difference between the products and reactants enthalpies for complete combustion at a given temperature and pressure, property that is represented by the equation 3.13 [33].

$$h_{RP} = \sum_P n h - \sum_R n h \quad (3.13)$$

where:

n is the number of moles

h is the enthalpy

The heating value of the gas products can be calculated with the same approach, using equations 3.13 and 3.11. However, the LHV values for gases are commonly present on thermodynamic tables. Therefore, tabled values were used from Shapiro et al. [33].

The heating value of the product yields are then given by Eq 3.14.

$$LHV_{\text{liq, gas}} = \sum_{\text{sp}} Y_{\text{sp}} LHV_{\text{sp}} \quad (3.14)$$

Relative Error

As it will be presented on the following chapter, there are various parameters that can be changed in the implemented kinetic scheme, therefore, to track the effectiveness of the modifications is crucial. The best option is the one with a less accentuated deviation from the experimental data.

In order to account the magnitude of the deviations, the relative error is used. The considered parameters for the relative error are the following:

- Value of mass loss rate peak (TGA) and temperature at which occurs; this parameter allows to quantify the extension of the reactions that take place under a given temperature profile.
- Mass, liquid and gas yields; the generated products yields are relevant to quantify the volatile matter that goes to each phase.
- Gas composition; similarly to the yields, permits the quantification of each produced gas.
- Value of CO and CO₂ production rates peaks and temperature at which both occur; with the biggest gas contributions coming from CO and CO₂, the profile of the released gases present great relevance to predict the behaviour of devolatilization under an imposed temperature profile.

Taking into account all the parameters mentioned above, the relative error is given by Eq. 3.15.

$$Error = \sum_i \left| \frac{P_{i, \text{num}} - P_{i, \text{exp}}}{P_{i, \text{exp}}} \right| w_i \quad (3.15)$$

where:

$P_{i, \text{exp}}$ is the experimental value of parameter i .

$P_{i, \text{num}}$ is the numerical value of parameter i .

w_i is the weight of the given parameter.

3.2 Model Assumptions

The implemented model only accounts for the kinetics, as a consequence, the following assumptions were made:

- Temperature gradients inside the particle can be neglected due to the small size of the particles.
- Interactions between organic and inorganic components of biomass are neglected.
- The reactor has adiabatic and chemically-inert walls.

3.3 Kinetic scheme

The present section aims to explain the implemented torrefaction kinetic scheme which was adapted by Anca-Couce et al. [18], from a pyrolysis mechanism from Ranzi et al. [17]. Figure 3.2 shows the kinetic scheme from Ranzi et al. [34] for pyrolysis.

Pyrolysis Reactions			Kinetic Parameters A (s ⁻¹), Eact
Cellulose			
1	CELL	→ CELLA	$1.5 \times 10^{14} \times \exp(-47000/RT)$
2	CELLA	→ 0.4 HAA + 0.05 GLYOX + 0.15 CH ₃ CHO + 0.25 HMFU + 0.35 ALD3 + 0.15 CH ₃ OH + 0.3 CH ₂ O + 0.61 CO + 0.36 CO ₂ + 0.05 H ₂ + 0.93 H ₂ O + 0.02 HCOOH + 0.05 C ₃ H ₆ O ₂ + 0.05 G{CH ₄ }+	$2.5 \times 10^6 \times \exp(-19100/RT)$
3	CELLA	→ LVG	$3.3 \times T \times \exp(-10000/RT)$
4	CELL	→ 5 H ₂ O + 6 CHAR	$6 \times 10^7 \times \exp(-31000/RT)$
Hemicellulose			
5	GMSW	→ 0.70 HCE1 + 0.30 HCE2	$1 \times 10^{10} \times \exp(-31000/RT)$
6	XYHW	→ 0.35 HCE1 + 0.65 HCE2	$1 \times 10^{10} \times \exp(-28500/RT)$
7	HCE1	→ 0.6 XYLAN + 0.2 C ₃ H ₆ O ₂ + 0.12 GLYOX + 0.2 FURF + 0.4 H ₂ O + 0.08 G{H ₂ } + 0.16 CO	$3 \times T \times \exp(-11000/RT)$
8	HCE1	→ 0.4 H ₂ O + 0.79 CO ₂ + 0.05 HCOOH + 0.69 CO + 0.01 G{CO} + 0.01 G{CO ₂ } + 0.35 G{H ₂ } + 0.3 CH ₂ O + 0.9 G{COH ₂ } + 0.625 G{CH ₄ } + 0.375 G{C ₂ H ₄ } + 0.875 CHAR	$1.8 \times 10^{-3} \times T \times \exp(-3000/RT)$
9	HCE2	→ 0.2 H ₂ O + 0.275 CO + 0.275 CO ₂ + 0.4 CH ₂ O + 0.1 C ₂ H ₅ OH + 0.05 HAA + 0.35ACAC + 0.025 HCOOH + 0.25 G{CH ₄ } + 0.3 G{CH ₃ OH} + 0.225 G{C ₂ H ₄ } + 0.4 G{CO ₂ } + 0.725 G{COH ₂ }+	$5 \times 10^9 \times \exp(-31500/RT)$
Lignins			
10	LIGC	→ 0.35 LIGCC + 0.1 COUMARYL + 0.08 PHENOL + 0.41 C ₂ H ₄ + 1.0H ₂ O + 0.7 G{COH ₂ } + 0.3 CH ₂ O + 0.32 CO + 0.495 G{CH ₄ }+	$1 \times 10^{11} \times \exp(-37200/RT)$
11	LIGH	→ LIGOH + 0.5 ALD3 + 0.5 C ₂ H ₄ + 0.2 HAA + 0.1 CO + 0.1 G{H ₂ }	$6.7 \times 10^{12} \times \exp(-37500/RT)$
12	LIGO	→ LIGOH + CO ₂	$3.3 \times 10^8 \times \exp(-25500/RT)$
13	LIGCC	→ 0.3 COUMARYL + 0.2 PHENOL + 0.35 HAA + 0.7 H ₂ O + 0.65 CH ₄ + 0.6 C ₂ H ₄ + H ₂ + 1.4 CO + 0.4 G{CO} + 6.75 CHAR	$1 \times 10^4 \times \exp(-24800/RT)$
14	LIGOH	→ 0.9 LIG + H ₂ O + 0.1 CH ₄ + 0.6 CH ₃ OH + 0.05 G{H ₂ } + 0.3 G{CH ₃ OH} + 0.05 CO ₂ + 0.65 CO + 0.6 G{CO} + 0.05 HCOOH + 0.85 G{COH ₂ } + 0.35 G{CH ₄ } + 0.2 G{C ₂ H ₄ } + 4.25 CHAR+	$1 \times 10^8 \times \exp(-30000/RT)$
15	LIG	→ 0.7 FE2MACR + 0.3 ANISOLE + 0.3 CO + 0.3 G{CO} + 0.3 CH ₃ CHO	$4 \times T \times \exp(-12000/RT)$
16	LIG	→ 0.6 H ₂ O + 0.4 CO + 0.2 CH ₄ + 0.4 CH ₂ O + 0.2 G{CO} + 0.4 G{CH ₄ } + 0.5 G{C ₂ H ₄ } + 0.4 G{CH ₃ OH} + 2 G{COH ₂ } + 6 CHAR	$8.3 \times 10^{-2} \times T \times \exp(-8000/RT)$
17	LIG	→ 0.6 H ₂ O + 2.6 CO + 1.1 CH ₄ + 0.4 CH ₂ O + C ₂ H ₄ + 0.4 CH ₃ OH+	$1 \times 10^7 \times \exp(-24300/RT)$
Extractives			
18	TGL	→ ACROL + 3 FFA	$7 \times 10^{12} \times \exp(-45700/RT)$
19	TANN	→ 0.85 FENOL + 0.15 G{PHENOL} + G{CO} + H ₂ O + ITANN	$2 \times 10^1 \times \exp(-10000/RT)$
20	ITANN	→ 5 CHAR + 2 CO + H ₂ O + G{COH ₂ }	$1 \times 10^3 \times \exp(-25000/RT)$
Metaplastic			
21	G{CO ₂ }	→ CO ₂	$1 \times 10^6 \times \exp(-24000/RT)$
22	G{CO}	→ CO	$5 \times 10^{12} \times \exp(-50000/RT)$
23	G{COH ₂ }	→ CO + H ₂	$1.5 \times 10^{12} \times \exp(-71000/RT)$
24	G{H ₂ }	→ H ₂	$5 \times 10^{11} \times \exp(-75000/RT)$
25	G{CH ₄ }	→ CH ₄	$5 \times 10^{12} \times \exp(-71500/RT)$
26	G{CH ₃ OH}	→ CH ₃ OH	$2 \times 10^{12} \times \exp(-50000/RT)$
27	G{C ₂ H ₄ }	→ C ₂ H ₄	$5 \times 10^{12} \times \exp(-71500/RT)$
28	G{PHENOL}	→ PHENOL	$1.5 \times 10^{12} \times \exp(-71000/RT)$
H ₂ O Evap.			
29	ACQUA	→ H ₂ O	$1 \times T \times \exp(-8000/RT)$

Figure 3.2: Pyrolysis kinetic scheme from Ranzi et al. [34].

In Table 3.1 is the employed kinetic scheme for torrefaction where the detailed reactions can be seen. The kinetic scheme is influenced by the imposed temperature profile, biomass composition, x_i , y_{13} and Reaction 5, from Table 3.1, which varies accordingly to the biomass type. Torrefaction behaviour is considered to be the combination of each individual components [18, 25], thus, the presented reactions are shown for each individual component.

Table 3.1: kinetic scheme from Anca-Couce et al. [18], where y_{13} is defined by Eq. 3.16.

Reaction		A [s ⁻¹]	E [KJ/mol]	
1	CELL	$\rightarrow (1 - x_1) * (0.95 \text{ HAA} + 0.25 \text{ GLYOX} + 0.2 \text{ CH}_3\text{CHO} + 0.25 \text{ HMFU} + 0.2 \text{ C}_3\text{H}_6\text{O} + 0.16 \text{ CO}_2 + 0.1 \text{ CH}_4 + 0.61 \text{ Char}) + x_1 * (5.5 \text{ Char} + 4 \text{ H}_2\text{O} + 0.5 \text{ CO}_2 + \text{H}_2)$	8×10^{13}	192.5
5	HCE	$\rightarrow 0.4 * [(1 - x_5) * (0.75 \text{ GH}_2 + 0.8 \text{ CO}_2 + 1.4 \text{ CO} + 0.5 \text{ CH}_2\text{O} + 0.25 \text{ CH}_3\text{OH} + 0.125 \text{ ETOH} + 0.125 \text{ H}_2\text{O} + 0.625 \text{ CH}_4 + 0.25 \text{ C}_2\text{H}_4 + 0.675 \text{ Char}) + x_5 * (4.5 \text{ Char} + 3 \text{ H}_2\text{O} + 0.5 \text{ CO}_2 + \text{H}_2)] + 0.6 \text{ HCE2}$	1×10^{10}	129.7
5 (HW)	HCEHW	$\rightarrow 0.4 \text{ AA} + 0.4 * [(1 - x_5) * (0.75 \text{ GH}_2 + 0.8 \text{ CO}_2 + 1.4 \text{ CO} + 0.5 \text{ CH}_2\text{O} + 0.25 \text{ CH}_3\text{OH} + 0.125 \text{ ETOH} + 0.125 \text{ H}_2\text{O} + 0.625 \text{ CH}_4 + 0.25 \text{ C}_2\text{H}_4 + 0.675 \text{ Char}) + x_5 * (4.5 \text{ Char} + 3 \text{ H}_2\text{O} + 0.5 \text{ CO}_2 + \text{H}_2)] + 0.6 \text{ HCE2}$	$1 * 10^{10}$	129.7
5 (SW)	HCESW	$\rightarrow 0.1 \text{ AA} + 0.4 * [(1 - x_5) * (0.75 \text{ GH}_2 + 0.8 \text{ CO}_2 + 1.4 \text{ CO} + 0.5 \text{ CH}_2\text{O} + 0.25 \text{ CH}_3\text{OH} + 0.125 \text{ ETOH} + 0.125 \text{ H}_2\text{O} + 0.625 \text{ CH}_4 + 0.25 \text{ C}_2\text{H}_4 + 0.675 \text{ Char}) + x_5 * (4.5 \text{ Char} + 3 \text{ H}_2\text{O} + 0.5 \text{ CO}_2 + \text{H}_2)] + 0.6 \text{ HCE2}$	1×10^{10}	129.7
8	HCE2	$\rightarrow (1 - x_8) * (0.2 \text{ CO}_2 + 0.5 \text{ CH}_4 + 0.25 \text{ C}_2\text{H}_4 + 0.8 \text{ GCO}_2 + 0.8 \text{ GCOH}_2 + 0.7 \text{ CH}_2\text{O} + 0.25 \text{ CH}_3\text{OH} + 0.125 \text{ ETOH} + 0.125 \text{ H}_2\text{O} + \text{Char}) + x_8 * (4.5 \text{ Char} + 3 \text{ H}_2\text{O} + 0.5 \text{ CO}_2 + \text{H}_2)$	1×10^{10}	138.1
9	LIG-C	$\rightarrow 0.35 \text{ LIG-CC} + 0.1 \text{ pCOUMARYL} + 0.08 \text{ PHENOL} + 0.41 \text{ C}_2\text{H}_4 + \text{H}_2\text{O} + 0.495 \text{ CH}_4 + 0.32 \text{ CO} + \text{GCOH}_2 + 5.735 \text{ Char}$	4×10^{15}	202.9
10	LIG-H	$\rightarrow \text{LIG-OH} + \text{C}_3\text{H}_6\text{O}$	2×10^{13}	156.9
11	LIG-O	$\rightarrow \text{LIG-OH} + \text{CO}_2$	1×10^9	106.7
12	LIG-CC	$\rightarrow (1 - x_{12}) * (0.3 \text{ pCOUMARYL} + 0.2 \text{ PHENOL} + 0.35 \text{ C}_3\text{H}_4\text{O}_2 + 0.7 \text{ H}_2\text{O} + 0.65 \text{ CH}_4 + 0.6 \text{ C}_2\text{H}_4 + \text{GCOH}_2 + 0.8 \text{ GCO} + 6.4 \text{ Char}) + x_{12} * (14.5 \text{ Char} + 3 \text{ H}_2\text{O} + 0.5 \text{ CO}_2 + 4 \text{ H}_2)$	5×10^6	131.8
13	LIG-OH	$\rightarrow \text{H}_2\text{O} + \text{CH}_3\text{OH} + 0.45 \text{ CH}_4 + 0.2 \text{ C}_2\text{H}_4 + 1.4 \text{ GCO} + 0.6 \text{ GCOH}_2 + 0.1 \text{ GH}_2 + 4.15 \text{ Char} + [(1 - x_{13}) * (y_{13} * \text{FE2MACR} + (1 - y_{13}) * (\text{H}_2\text{O} + 0.5 \text{ CO} + 0.2 \text{ CH}_2\text{O} + 0.4 \text{ CH}_3\text{OH} + 0.2 \text{ CH}_3\text{CHO} + 0.2 \text{ C}_3\text{H}_6\text{O} + 0.6 \text{ CH}_4 + 0.65 \text{ C}_2\text{H}_4 + \text{GCO} + 0.5 \text{ GCOH}_2 + 5.5 \text{ Char})) + x_{13} * (10.5 \text{ Char} + 3 \text{ H}_2\text{O} + 0.5 \text{ CO}_2 + 3 \text{ H}_2)]$	3×10^8	125.5
16	GCO ₂	$\rightarrow \text{CO}_2$	1×10^5	100.4
17	GCO	$\rightarrow \text{CO}$	1×10^{30}	209.2
18	GCOH ₂	$\rightarrow \text{CO} + \text{H}_2$	5×10^{11}	272.0
19	GH ₂	$\rightarrow \text{H}_2$	5×10^{11}	313.8

$$y_{13}(T) = (-3.6800 \times 10^{11} T^5 + 8.2619 \times 10^8 T^4 - 6.8901 \times 10^5 T^3 + 2.6124 \times 10^2 T^2 - 4.5911 T + 4.0398 \times 10^2) / 100 \quad (3.16)$$

where:

T is the temperature in [°C].

The presented scheme from Table 3.1, was adapted to include the presence of secondary char formation reactions, which corresponds to the x_1 parameter. In regards to the reactions of each component, cellulose is described with one reaction representing devolatilization through ring fragmentation [18], additionally, the secondary reactions which represent charring, are represented by x_1 . These parameter x_1 , quantifies the release of primary products through fragmentation of the rings [18], the released products then react to form secondary products. In opposition to to cellulose, the thermal decomposition of lignin is a combination of three different components, LIG-C, LIG-H and LIG-O, as these have a higher content of carbon, hydrogen and oxygen respectively. On these reactions, specifically on reaction 13, a parameter y_{13} is shown and its effect will be latter analysed and discussed. The parameter x_1 is adjustable,

although, its suggested value is 0.3 for woody biomass for the tested temperatures by Anca-Couce et al. [18]. This parameter might be influenced by the imposed temperatures and biomass composition. Lastly, the presented reaction that describes hemicellulose thermal degradation consists of two successive reactions, reaction 5 and 8 from Table 3.1. The reaction for hemicellulose is based on pyrolysis of xylan, which accurately describes the hemicelluloses of hardwood, but the same might not apply for non-woody biomass types, and softwoods.

Going further deep into reaction 5, hemicellulose is described by there different reactions as a function of the biomass type in use, which are described as it follows:

- $\text{HCE} \rightarrow 0.4 \text{ HCE1} + 0.6 \text{ HCE2}$
- $\text{HCESW} \rightarrow 0.1 \text{ AA} + 0.4 \text{ HCE1} + 0.6 \text{ HCE2}$
- $\text{HCEHW} \rightarrow 0.4 \text{ AA} + 0.4 \text{ HCE1} + 0.6 \text{ HCE2}$

where:

AA is Acetic Acid.

HCE1 is the hemicellulose depolymerization reaction.

HCE2 is the hemicellulose ring opening reaction.

The presence of acetic acid constitutes an attempt to better describe the generated products, accordingly to the biomass type. Different hemicellulose polysaccharides lead to different products and concentrations. The author of the given kinetic scheme opted to diminish the differences between biomass types by adapting reaction 5 to meet the generated product.

As mentioned previously in section 2.1, hardwood is better described as acetyl glucuronoxylan [23], which is composed by 10 xylose molecules, 7 acetyl groups and 1 glucuronic acid [35], where the acetyl groups made out around 15% of the mass. Therefore, the kinetic scheme tries to account for the presence of this acetyl groups by adding 4 acetic acid molecules per 10 of xylan molecules. This results in the same weight percentage of acetyl groups. Similarly, the same was done for softwood. Softwood is mainly composed by galactoglucomannans, glucomannan and arabinoglucuronoxylan [35, 36]. Glucomannan composition consists on 4 hexose sugar monomers and 1 acetyl group [35], which represent 4.5 % of the total mass. Hence, per 10 xylan molecules there is 1 acetic acid molecule, so it accounts for 4.5% of the mass. However, acetylation greatly varies in softwood which causes uncertainties [18].

Nevertheless, this adaptation proved not be suitable since the reactions with acetic acid do not assure the mass balance. Since the molar coefficients of HCE1 and HCE2 were not adjusted, the model could not use the reactions representative of each biomass type. Reaction 5, without acetic acid was the chosen reaction to implement since it was the only one where the mass balance was achieved.

On the other hand, a study conducted by Dussan et al. [37], which replicated the chemical structure of hardwood, softwood and herbaceous biomass using xylan cluster (xylan with acetyl and 4-methyl-D-glucuronic acid groups), arabinoxylan, xyloglucan, glucomannan and β -glucan for pyrolysis, provided better predictions on the char and volatile yields. Since the study indicates that the distinction between

different hemicellulose types provided better predictions, it served as a solid base for Debiagi et al. [19] to suggest different combinations of HCE1 and HCE2 coefficients in order to replicate the different biomass types. Debiagi et al. [19] concluded that hemicellulose in softwood can be represented by $HCE1/HCE2 = 70/30$, hardwood by $HCE1/HCE2 = 35/65$ and herbaceous biomass by $HCE1/HCE2 = 12/88$. This suggests that the ratio of HCE1/HCE2 can be changed in order to accommodate different biomass types. Therefore, this has become a valid variable parameter to be explored further on.

Lastly, reactions 16-19 from Table 3.1 represent by G before the species name, are pseudo-species trapped in the metaplastic phase that are progressively released, through secondary reactions at higher temperatures [38]. These reactions are not typically active at torrefaction temperatures [18].

Chapter 4

Model adaptations and Results

The present section aims to compare the results obtained from the implemented torrefaction kinetic scheme from Anca-Couce et al. [18], presented on Table 3.1, against an adaptation of the same model, a pyrolysis kinetic scheme [34] and experimental data.

Experimental data

The experimental data was obtained for a sample of nut shell, which composition can be seen on Table 4.1 provided by the database from Debiagi et al. [19]. On Table 4.2 is presented the proximate and ultimate analysis for the same sample. The ultimate analysis of each sample was performed using a CHN 2000 LECO analyzer following the standards ASTM D5373. Oxygen was computed by difference. The proximate analysis was performed using a TGA701 LECO thermogravimetric analyzer with a resolution of 0.1 mg, following the standard D5142.

Table 4.1: Biomass composition in wt. % from nut shell sample.

	Nut shell
Cellulose	29.25
Hemicellulose	26.64
LIG-C	9.36
LIG-H	23.27
LIG-O	2.46
TGL	2.83
TANN	5.98

Table 4.2: Biomass proximate and ultimate analysis, in wt. % dry from nut shell sample.

Proximate analysis (wt. %, dry)	Nut shell
Volatile Matter	79.66
Fix Carbon	20.03
Ash	0.31
Ultimate analysis (wt. %, dry)	
Carbon	42.50
Hydrogen	5.97
Oxygen	51.42
Nitrogen	0.11

The product yields, gas composition and its formation rates were obtained, using the temperature profile "Reactor Profile" from Figure 4.1. The reactor is constituted by a jacketed prismatic chamber including supports for five sample trays. In each one of them 1.5 g of biomass was placed in a very thin layer (1 mm) to avoid thermal gradients. The tests were carried out from room temperature up to 244 °C with a constant heating rate of 5 °C/min, and remained constant at 232 °C for approximately 13 minutes. The tests were conducted under atmospheric pressure and inert atmosphere of nitrogen. The volatiles produced in the reaction unit entered the condensation device, which consists of a jacketed coil. The stream of nitrogen drives the non condensable gases from the condenser to the gas sampling point. At the condenser's outlet, a catch pot submerged in a 273 K thermostatic bath collected the condensed volatiles. Permanent gases flowed into a silica gel trap, where the moisture content was reduced before they were sampled and analyzed. The gas composition, in terms of the volume percentage of the major gas species (CO, CO₂, H₂, CH₄, C₂H₆, N₂, and O₂), was measured every 171.5 s by a gas chromatograph equipped with a thermal conductivity detector (Agilent 3000 Quad). The bio-oil yield was obtained by difference.

The thermogravimetric tests were obtained in a 7200 Simultaneous Thermal Analyzer under an atmosphere of nitrogen. The samples were placed in a measuring crucible with an initial weight of about 1.5 mg. The sensitivity of the balance is $\pm 0.1 \mu\text{g}$ and the accuracy is better than 0.02%. The samples were heated from room temperature to 241 °C at a constant heating rate of 5 °C/min, and remained at the constant temperature of 241 °C for approximately 20 minutes, represented by "TGA Profile" from Figure 4.1. The precision of the temperature measurements is ± 2 °C.

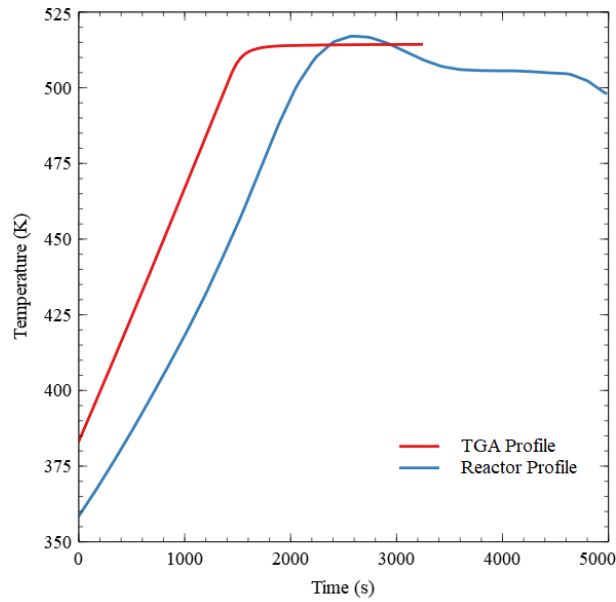


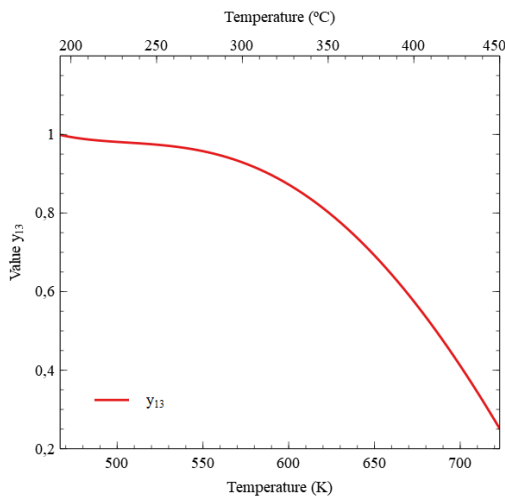
Figure 4.1: Used temperature profiles on experimental setup to obtain TGA (TGA Profile) and the profile of the released gases (Reactor Profile).

4.1 Model Adaptations

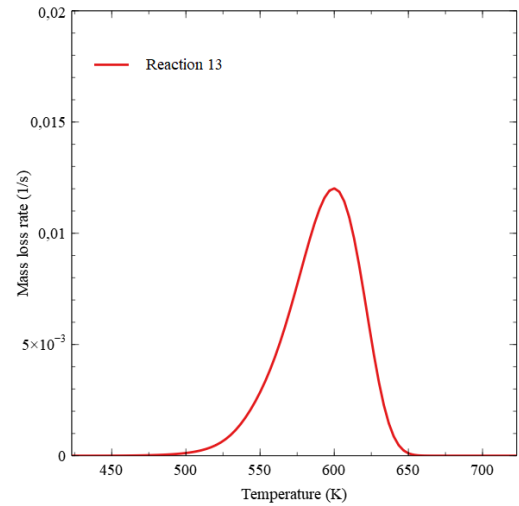
Previously on Section 3.3 it was mentioned the kinetic scheme is influenced by the imposed temperature profile, biomass composition, x_i , y_{13} and Reaction 5. The adopted temperatures profiles and biomass composition, are the ones from Figure 4.1 and Table 4.1, respectively, since it was the used conditions from which experimental data was obtained from. The influence of the remaining parameters is presented bellow.

Influence of y_{13} under torrefaction

From Chapter 2 it was mentioned that torrefaction over 300 °C is possible, but causes to much devolatilization, which is undesired. For the purpose of the present work, which uses torrefaction as a pre-treatment for gasification, the used temperatures are around 244 °C (517 K), which is bellow the 300 °C mark. The parameter, y_{13} , is given by Eq. 3.16, which is presented bellow and it is plotted in Figure 4.2.



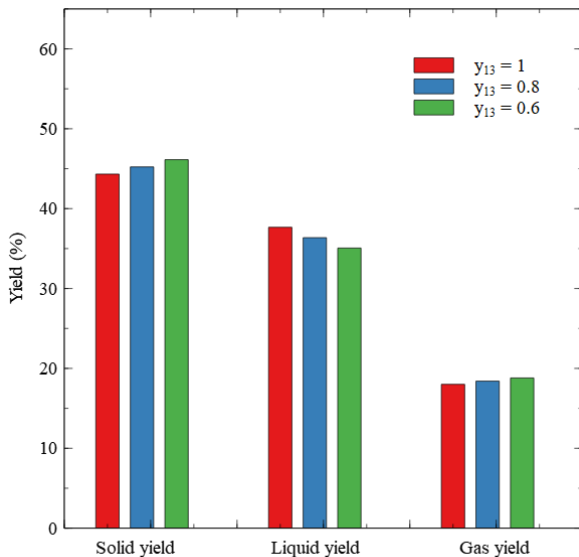
(a)



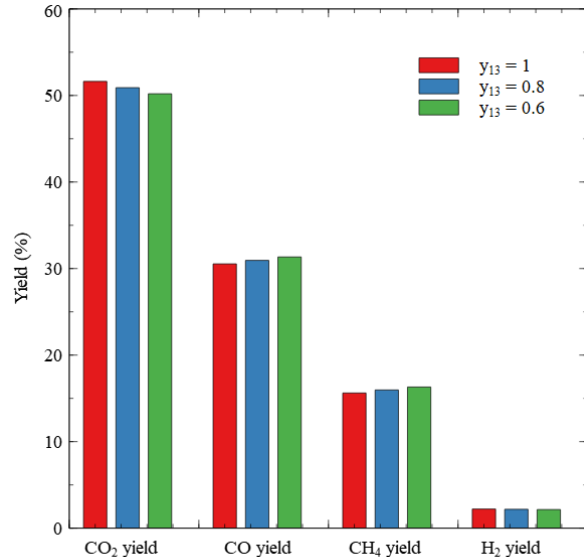
(b)

Figure 4.2: Value of y_{13} as a function of temperature (a) and reaction rate of reaction 13 from kinetic scheme presented on Table 3.1 as a function of the temperature (b).

From Figure 4.2, it can be seen that y_{13} values range from 1 to 0.25. However, observing the reaction rate of reaction 13, from the same Figure, the reaction starts at approximately at 500 K (227 ° C) and it is slightly over before 650 K (377 ° C). This means the parameter y_{13} has no effect outside the mentioned temperature range, where its corresponding value varies from 0.96 to 0.69. Nevertheless, a sensibility study was conducted at 300 ° C to better understand the influence of y_{13} under typical torrefaction temperatures. Presented on Figure 4.3 are the effects y_{13} had on product yields and gas composition.



(a)



(b)

Figure 4.3: Influence of y_{13} on the product yields at 300 ° C (a) and gas composition at 300 ° C (b).

Table 4.3 shows the product yields as a function of y_{13} values and the maximum deviation for each parameter.

Table 4.3: Deviations from sensibility test to y_{13} .

	Solid yield (%)	Liquid yield (%)	Gas yield (%)	CO ₂ (%)	CO (%)	CH ₄ (%)	H ₂ (%)
$y_{13} = 1$	44.3	37.7	18.0	51.6	30.5	15.6	2.2
$y_{13} = 0.8$	45.2	36.4	18.4	50.9	30.9	16.0	2.2
$y_{13} = 0.6$	46.1	35.1	18.8	50.2	31.3	16.3	2.2
Maximum deviation	1.8	2.6	0.8	1.4	0.8	0.7	0

The realist behaviour of the tested parameter, y_{13} , would be a gradual progression of its value as the temperature increases. Fixing the value translates into bigger deviations since it is set for the entirety of the reaction extension, amplifying the deviations. Regardless, from Table 4.3 the most significant deviations come from the liquid yield, solid yield and CO₂ yield which are still considered small, for the temperatures which will be used for the pre-treatment such extreme values of y_{13} will not be reached, diminishing the potential for error contribution. Taking all of this into account, y_{13} has little to no influence on torrefaction, therefore, will not be accounted as a changeable parameter, being so, its value is fixed at 1.

Influence of x_i and HCE1/HCE2

In order to better understand the influence of x_i and HCE1/HCE2 ratios, which, as mentioned in Section 3.3 can replicate different types of hemicellulose, the relative error was calculated using Eq. 3.15 and it is shown in Figure 4.4.

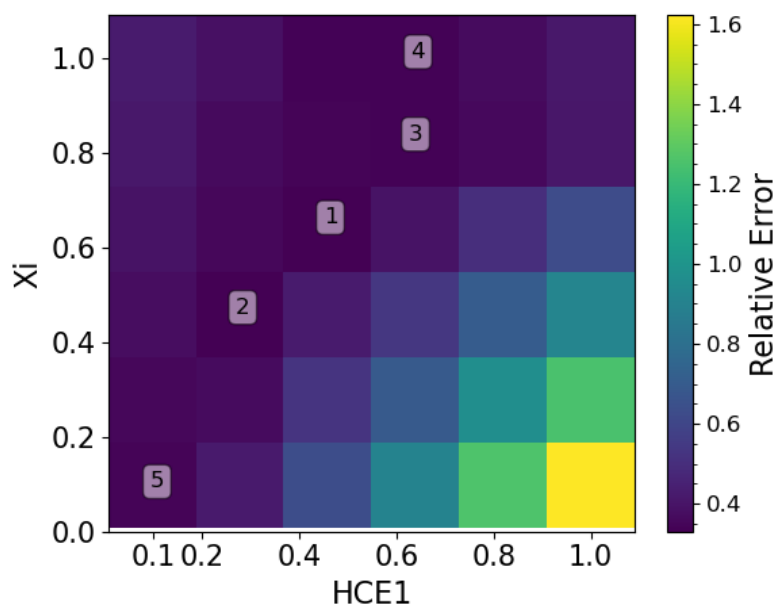


Figure 4.4: Relative error as a function of x_i and HCE1, where cells 1 to 5 represents the smallest errors in increasing order.

From Figure 4.4 the relative error is greater for higher values of HCE1 and lower values of x_i , which

represents a higher extension of hemicellulose depolymerization and less ring opening reaction, along with lower amount of secondary reactions which form secondary products as char, H₂O, CO₂ and H₂ [18]. There is a tendency, where the increase of HCE1 along with the increment of secondary reactions favours better results. However, the increment of HCE1 without the increase of x_1 causes large deviations.

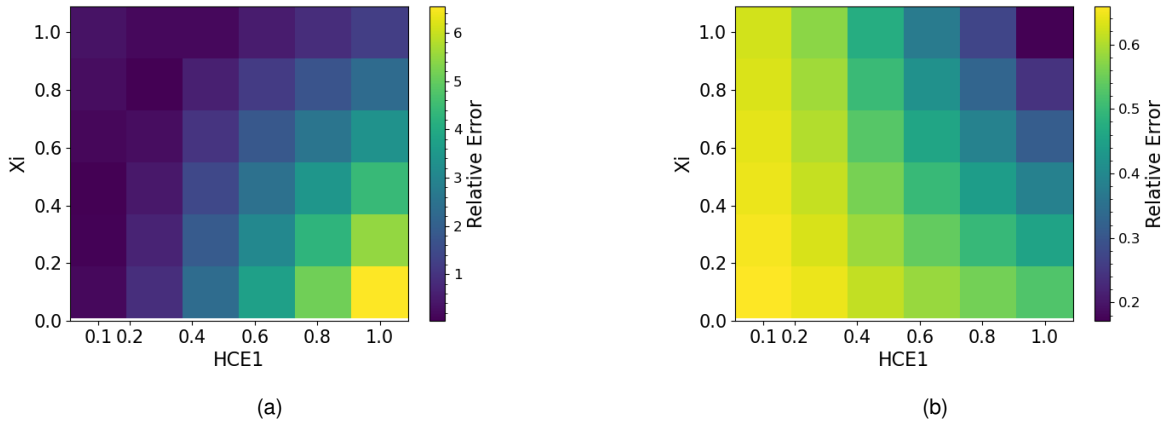


Figure 4.5: Relative error of gas yield (a) and liquid yield (b) as a function of x_1 and HCE1.

The Figure 4.5 presented above, show two considerable contributions for the relative error, the gas and liquid yields. The magnitude of the relative error for gas yields represents the largest contributor for the overall deviations. Lower values of HCE1 and higher values of x_1 provide a better prediction on gas yield. On the other hand, the relative error for liquid yields displays the opposite tendency, where the smallest error is favoured by higher values of HCE1, and also higher values of x_1 . The disparity between the tendencies imply a compromise between both parameters.

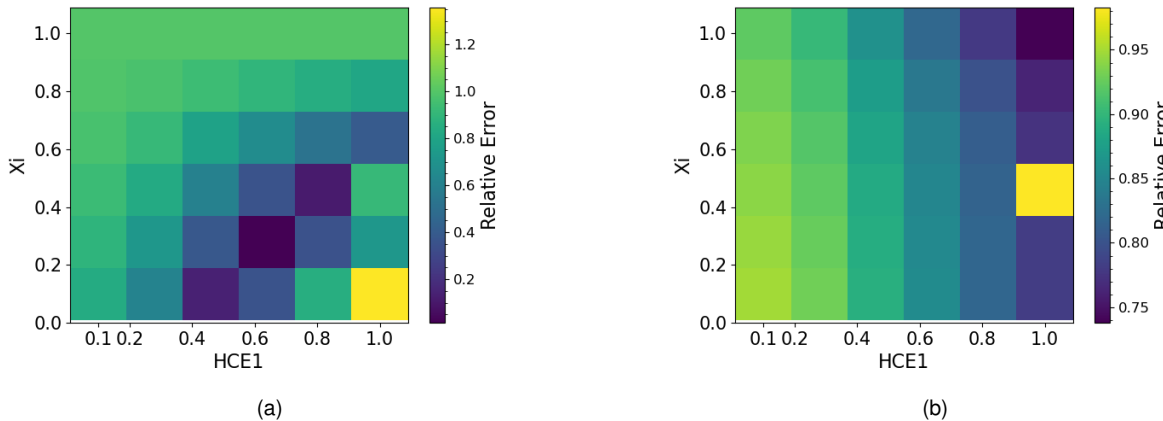


Figure 4.6: Relative error of CO yield (a) and CO₂ yield (b) as a function of x_1 and HCE1.

Similarly to the figures discussed before, the CO and CO₂ yields have a large contribution to the overall relative error. From Figure 4.6 it can be seen that the magnitude of the errors from CO yield have a larger contribution, over CO₂ yield, for the overall deviations. The best results for CO yield are favoured

by an increase on HCE1 followed by an increase in the amount of secondary reactions. On the contrary, CO₂, despite following the same tendency, the range which provides the best results is different, leading to a compromise between the yields.

Taking all the contributions into account, from Figure 4.4, the point which resulted in the lowest relative error is point 1, which corresponds to $x_i = 0.6$ and HCE1/HCE2 = 0.4/0.6, therefore, this point will be further adapted in order to optimize the results against experimental data.

Reactions adaptations

Gas composition is one of the fields where the implemented model from Anca-Couce et al. [18] deviates greatly from the experimental results. The kinetic scheme releases both CH₄ and C₂H₄ for the imposed temperature profiles which is not accurate, since the experimental tests did not detect those species. This means that CH₄ and C₂H₄ are not released for the tested temperatures, therefore, they must be only released at higher temperatures [19]. In order to account for this effect, reaction 5 from Table 3.1, which has the highest contribution to CH₄ formation, had the species CH₄ changed to GCH₄. The same principle was applied to C₂H₄, where, reactions 5 and 8 from Table 3.1, had the species C₂H₄ changed to GC₂H₄. The kinetic scheme has now to account for the new added species, which correspond to reactions 20 and 21 from Table 4.4.

As mentioned in Section 3.3, Anca-Couce et al. [18] attempted to account for the presence of acetic acid, but the adaptations did not ensure the mass balance of the reactions. Tumorulu et al. [3], also reported the presence of acetic acid in the product yields, with values between 2 and 5 % for the tested temperatures. The introduction of acetic acid was done in reaction 5 adapted from Table 4.4, resulting in the production of 4%. The introduction of acetic acid improves the liquid yields, although the molar coefficients of the generated liquids do need further adjustments as the predictions are only qualitative.

In regards to the kinetic parameters, reaction 11 from Table 4.4, along with reaction 5, are the largest contributors for CO and CO₂ production, which is shown in Figure 4.7. The kinetic parameters of reaction 11 were slightly adjusted to fit better the experimental CO₂ release rate. However, modifying the kinetic parameters of reaction 5 would affect both CO and CO₂ release rates, since CO₂ and CO rates would need to increase or decrease, respectively, this parameter could not be modified without compromising one of the rates.

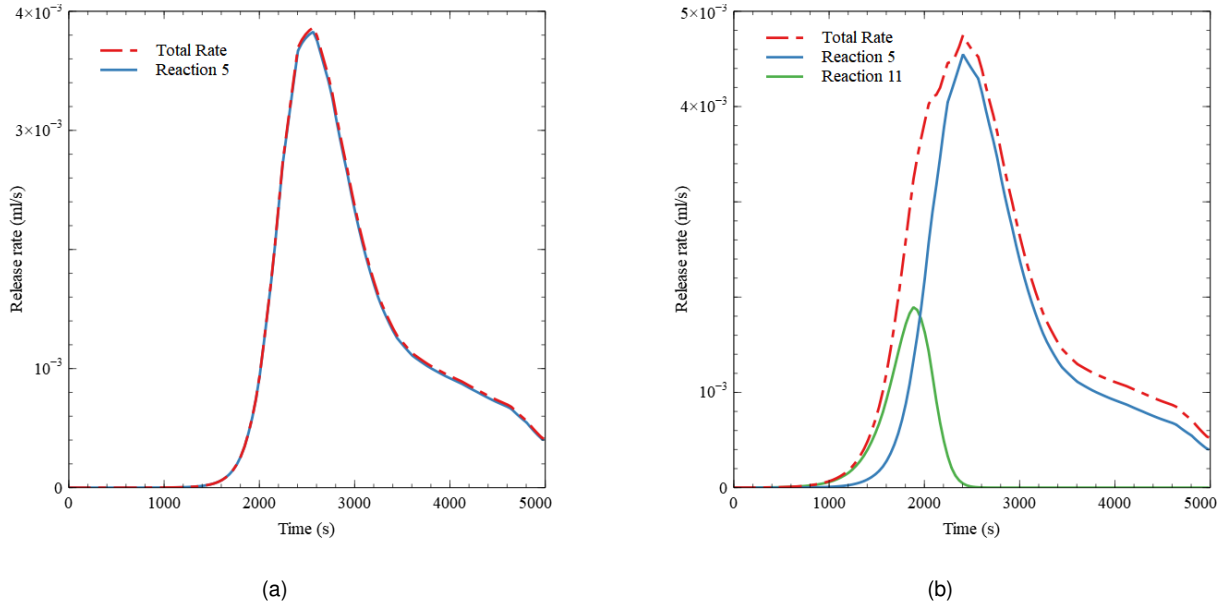


Figure 4.7: Contributions of reactions to the total release rate of CO (a) and CO₂ (b).

The Table 4.4 presented bellow, shows the adaptations made to the kinetic scheme, in comparison to the kinetic scheme from Table 3.1, with $x_i = 0.6$.

Table 4.4: kinetic scheme adaptation.

Reaction			A [s ⁻¹]	E [Kj/mol]
5	HCE	→ 0.04 C2H4 + 0.02 C2H5OH + 0.08 CH2O + 0.04 CH3OH + 0.1 CH4 + 1.188 CHAR + 0.224 CO + 0.248 CO2 + 0.12 GH2 + 0.24 H2 + 0.74 H2O + 0.6 HCE2	1 × 10 ¹⁰	129.7
5 Adapted	HCE	→ 0.04 GC2H4 + 0.02 C2H5OH + 0.08 CH2O + 0.04 CH3OH + 0.1 GCH4 + 1.108 CHAR + 0.04 CH3COOH + 0.224 CO + 0.248 CO2 + 0.12 GH2 + 0.24 H2 + 0.66 H2O + 0.6 HCE2	1 × 10 ¹⁰	129.7
8	HCE2	→ 0.1 C2H4 + 0.05 C2H5OH + 0.28 CH2O + 0.1 CH3OH + 0.2 GCH4 + 3.1 CHAR + 0.7 CO2 + 0 GCO2 + 0.32 GCOH2 + 0.6 H2 + 1.85 H2O	1 × 10 ¹⁰	138.1
8 Adapted	HCE2	→ 0.1 GC2H4 + 0.05 C2H5OH + 0.28 CH2O + 0.1 CH3OH + 0.2 GCH4 + 3.1 CHAR + 0.38 CO2 + 0.32 GCO2 + 0.32 GCOH2 + 0.6 H2 + 1.85 H2O	1 × 10 ¹⁰	138.1
11	LIG-O	→ LIG-OH + CO ₂	1 × 10 ⁹	106.7
11 Adapted	LIG-O	→ LIG-OH + CO ₂	2 × 10 ¹⁰	119.2
20	GCH ₄	→ CH ₄	5 × 10 ¹²	313.8
21	GC ₂ H ₄	→ GC ₂ H ₄	5 × 10 ¹²	313.8

4.2 Kinetic schemes comparison

The present section provides the comparison between the different kinetic schemes and its deviations in regards to the experimental data.

The Figure 4.8 presented bellow, shows the thermogravimetric analysis under the imposed temperature, TGA profile, from Figure 4.1 and the response of the different kinetic schemes.

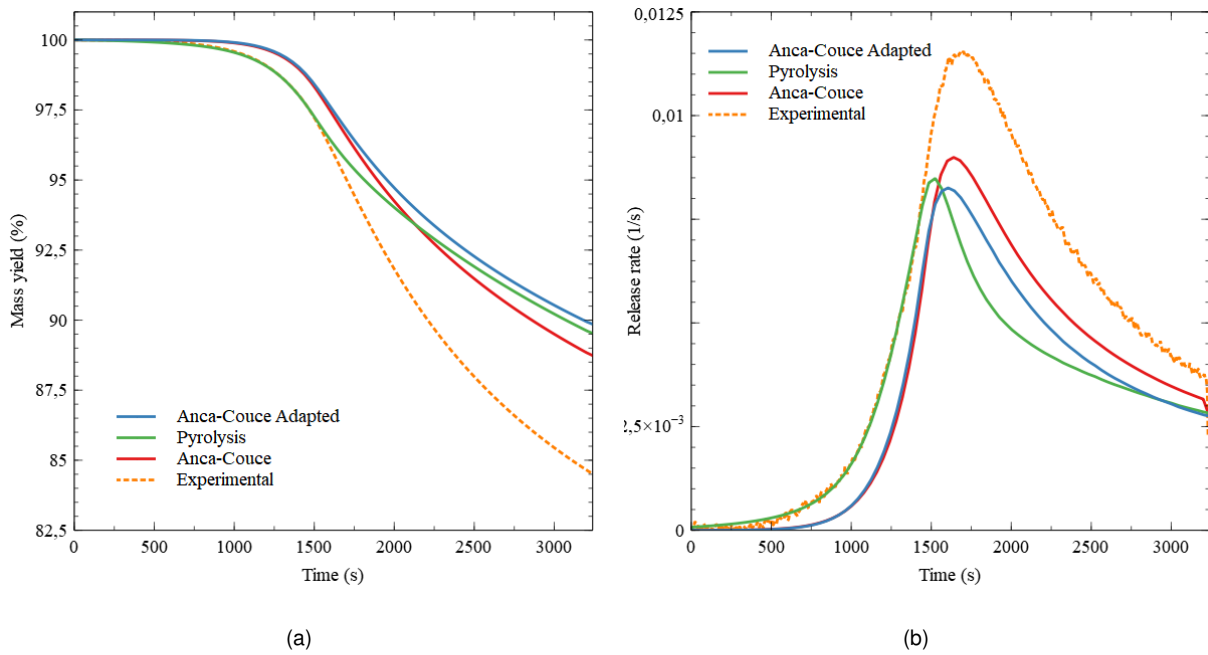


Figure 4.8: Mass yield profile (a) and respective rate (TGA) (b).

From Figure 4.8 all of the tested kinetic schemes under-predict the final mass yield and release rates. The peak in the release rate profile of both Anca-Couce and Anca-Couce adapted occur for later when compared to pyrolysis, which provides better prediction to when the releases occur. The difference in rates between the Anca-Couce and Anca-Couce adapted might be explained, not only by the amount of secondary reactions but also the adaptation of the pseudo-species, which might compromise the solid yield prediction in order to improve the gas composition.

Figure 4.9 shows the reaction production rates of both CO and CO₂, under the imposed temperature profile, Reactor profile, from Figure 4.1.

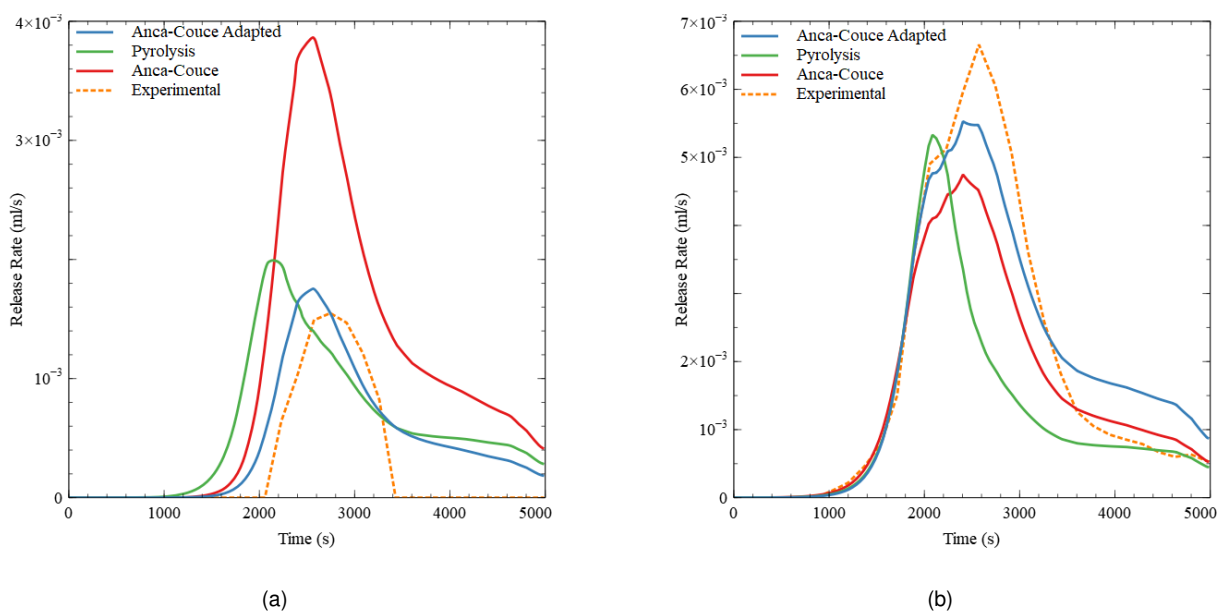


Figure 4.9: Release rates of CO (a) and CO₂ (b).

From Figure 4.9 presented above, it can be seen that the release rate for CO and CO₂ occurs early in pyrolysis, meaning that the rate peak occurs for lower temperatures than expected. The model from Anca-Couce is more accurate to when the peaks occurs in both CO and CO₂ release rates, although it over predicts the released amount of CO and under predicts the amount of CO₂. The adapted model, out of the three, is the one which presents the best prediction in regards to the profile of the released gases.

The Figure 4.10 shows, for the imposed temperature profile, Reactor profile, from Figure 4.1, the resultant product yields and gas composition. As it can be seen, the adapted model presented the best predictions on gas composition out of all the tested kinetic schemes. However, it still presents large deviations to the experimental data.

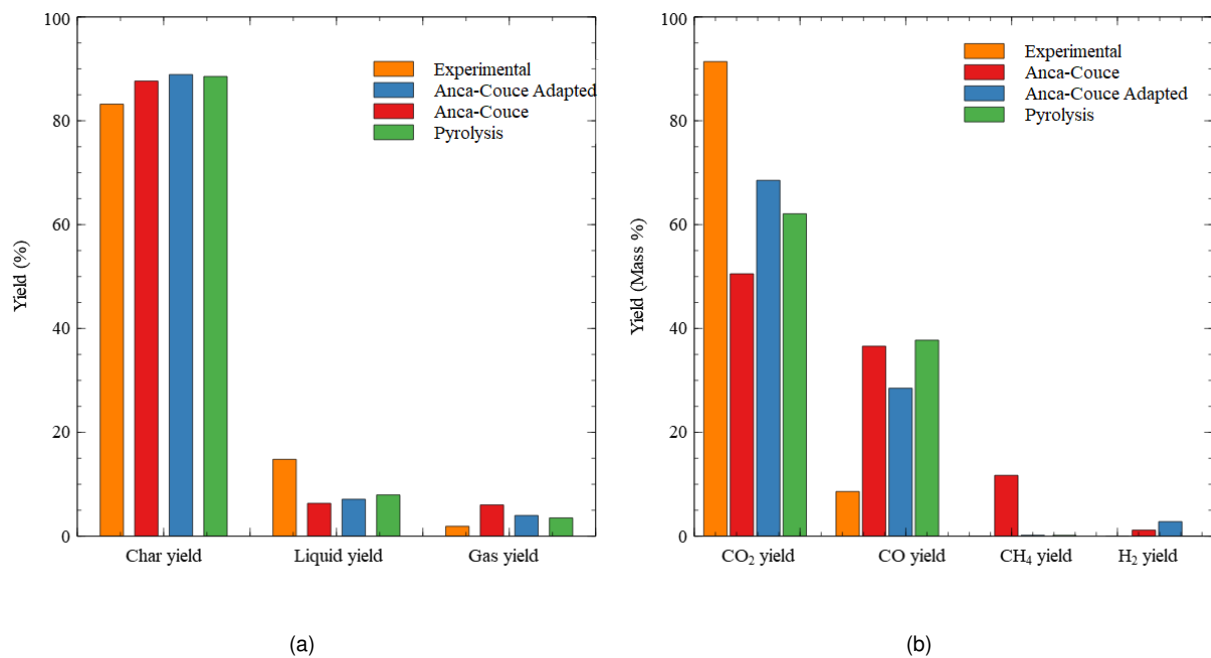


Figure 4.10: Product yields (a) and gas composition (b).

Table 4.5 presented below, shows the most significant deviations in regards to the experimental data, where the Error accounts for all of the error contributors described on Chapter 3, by Eq. 3.15.

Table 4.5: Deviations from the experimental results.

	Solid yield (%)	Liquid yield (%)	Gas yield (%)	CO ₂ (%)	CO (%)	Error (%)
Pyrolysis [34]	6.4	46.3	85.1	32.1	338.9	35.7
Anca-Couce	5.3	57.2	216.9	44.7	325.4	50.2
Anca-Couce Adapted	6.9	51.9	110.0	25.0	231.3	33.1

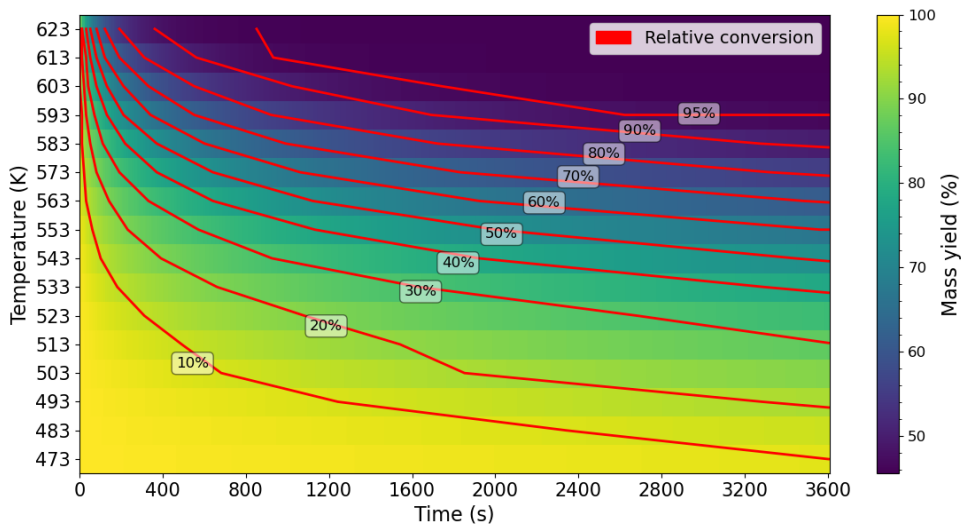
Some of the deviations in the yields of CO and CO₂ might be explained due to the small presence of O₂ in the reactor during the collection of the experimental data. The presence of O₂ can cause partial combustion, compromising the gas composition since it promotes the release of CO₂. Regarding the

opposite tendencies shown by the liquid and gas yields, along with its deviations, the kinetic scheme by Anca-Couce et al. [18] needs to be restructured to better predict the released species. Nevertheless, despite some large deviations regarding the characterisation of devolatilization, as it can be seen on Table 4.5, the adapted model has limited accuracy still provides the best behaviour under torrefaction as a pre-treatment for gasification out of the tested kinetic schemes.

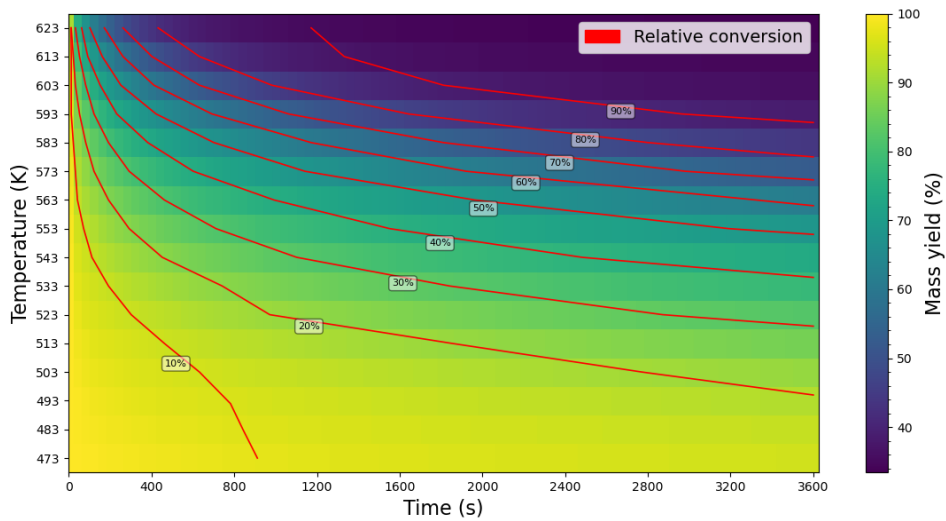
4.3 Parametric Study

This section aims to compare some of the points of interest (described in section 3.1.3) between the pyrolysis kinetic scheme, shown in Appendix A, and the adapted model.

Figure 4.11 represents the evolution of the mass yield as a function of the temperature and residence time. It can be seen that for lower temperatures the mass is preserved to a greater extent, whereas the mass yield decreases as the temperature and/or residence time increase. For the lowest temperature, 473K, for a residence time of 1h, the mass yield is greater than 95%, whereas for the highest temperature, 623K, for the same residence time, only 35% of the mass remains on the biomass for the pyrolysis reaction scheme. In regards to the adapted model, for the lowest temperature, 473K, for a residence time of 1h, the mass yield is also greater than 95%, whereas for the highest temperature, 623K, for the same residence time, 56% of the mass remains in biomass. On the same figure, represented by the red lines, is the percentage of relative conversion, which is the conversion achieved when compared the maximum conversion possible for the given temperature. The condition for achieving equilibrium was set as a change smaller than 1% over a 12 hour period. The pyrolysis maximum conversion varies from 73 %, for the lowest temperature, to 28 % for the highest temperature, whereas the adapted model varies from 72 %, for the lowest temperature, to 43 % for the highest temperature.



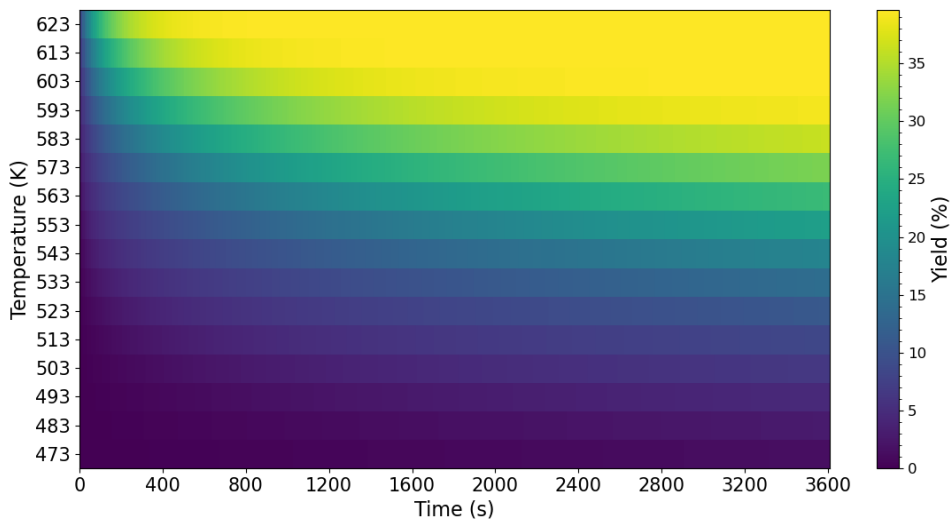
(a)



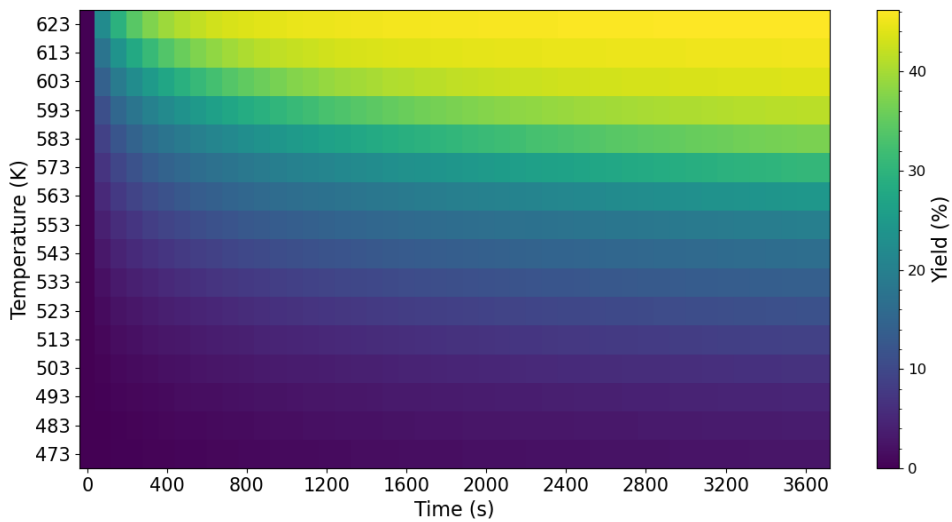
(b)

Figure 4.11: Mass evolution of the mass yield as a function of the temperature and residence time for the adapted model (a) and pyrolysis (b).

Represented on Figure 4.12 is the evolution of the liquid yield as a function of the temperature and residence time. In both cases the liquid yields are favoured by a longer residence time and higher temperatures, as mentioned in Chapter 2. Pyrolysis predicts more liquid formation over the adapted model under the tested temperatures, qualitatively both kinetic schemes behave the same way.



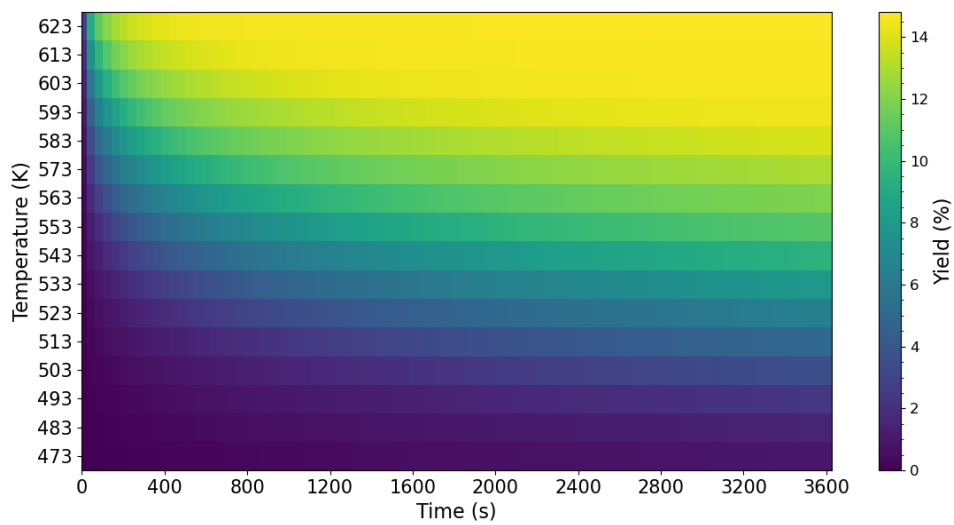
(a)



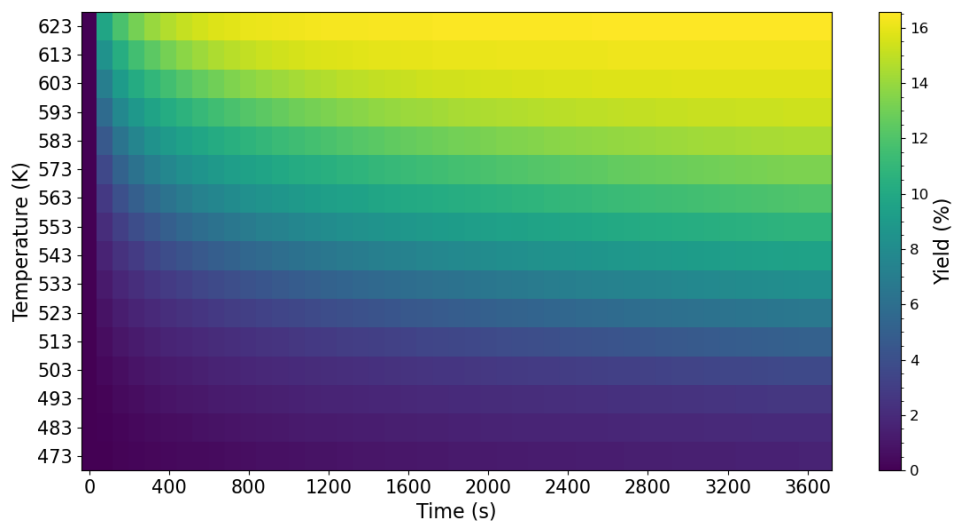
(b)

Figure 4.12: Liquid yield as a function of the temperature and residence time for the adapted model (a) and pyrolysis (b).

On a similar note to the figure presented above, Figure 4.13 presents the evolution of the liquid yield as a function of the temperature and residence time. In both cases the gas yields are favoured by a longer residence time and higher temperatures, as mentioned in Chapter 2. The predictions are relatively close when both kinetic schemes are compared.



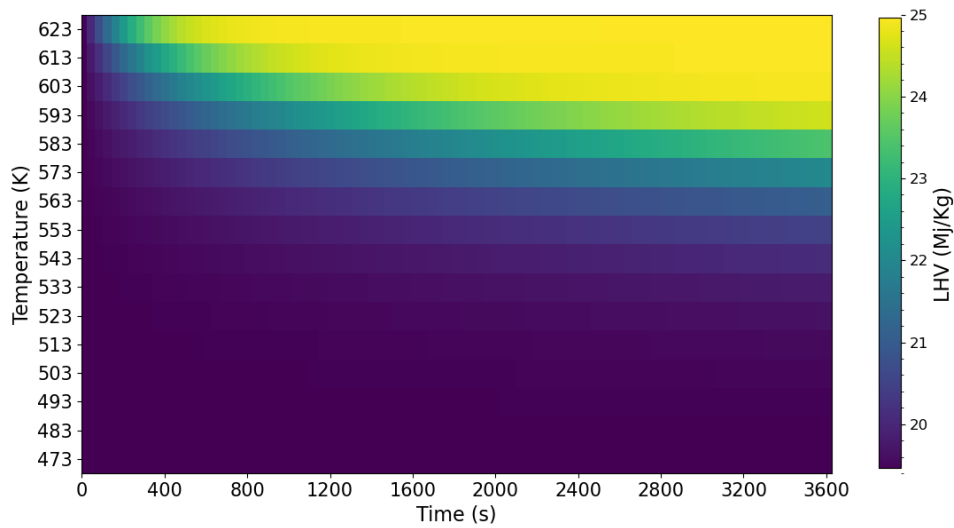
(a)



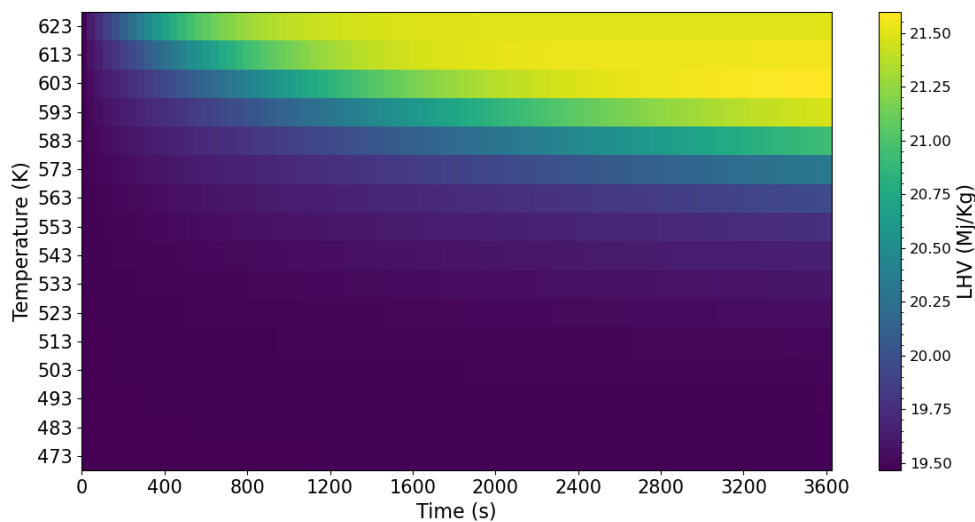
(b)

Figure 4.13: Liquid yield as a function of the temperature and residence time for the adapted model (a) and pyrolysis (b).

One of the most relevant values of interest is the heating values of torrefied biomass, since the increment in heating values adds value to biomass as fuels, as described previously on Chapter 1. The heating values of the torrefied biomass are presented below in Figure 4.14



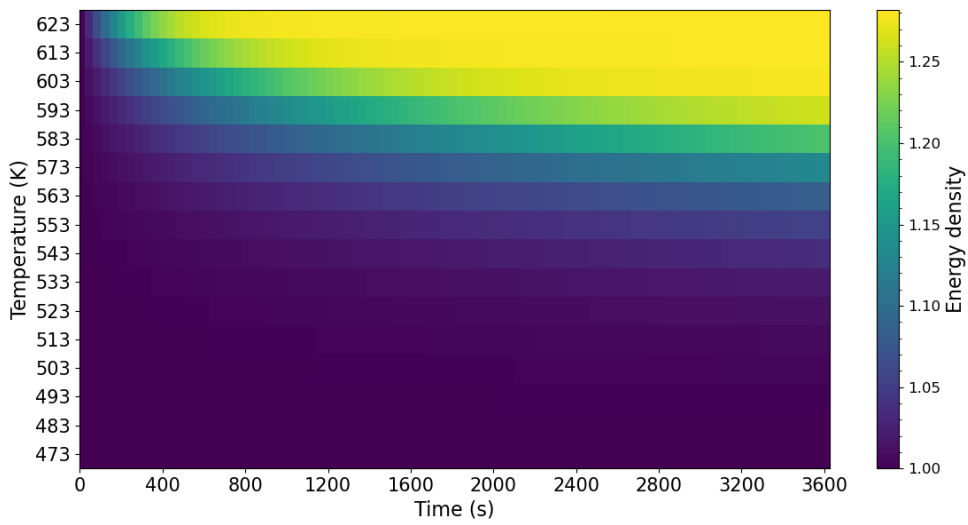
(a)



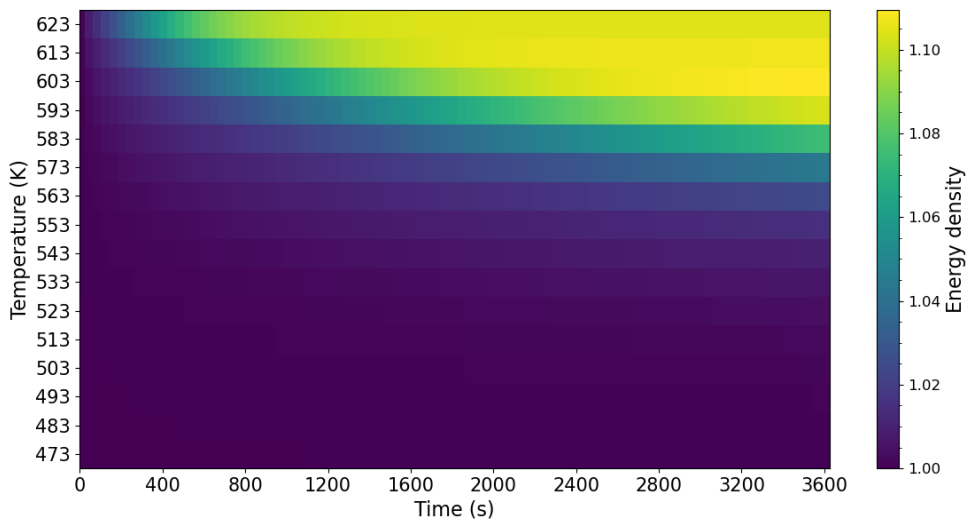
(b)

Figure 4.14: LHV as a function of the temperature and residence time for the adapted model (a) and pyrolysis (b).

From the Figure 4.14, it can be seen that the torrefied biomass increases its heating value as the temperature and residence time increase, the higher the temperature the less residence time is necessary to achieve the same conversion. This tendency goes into accordance with the literature presented previously, where Strandberg et al. [4] reported the same effect. The adapted model resulted in higher heating values, when compared to pyrolysis. This same figure can be better described by the energy densification which is shown below in Figure 4.15.



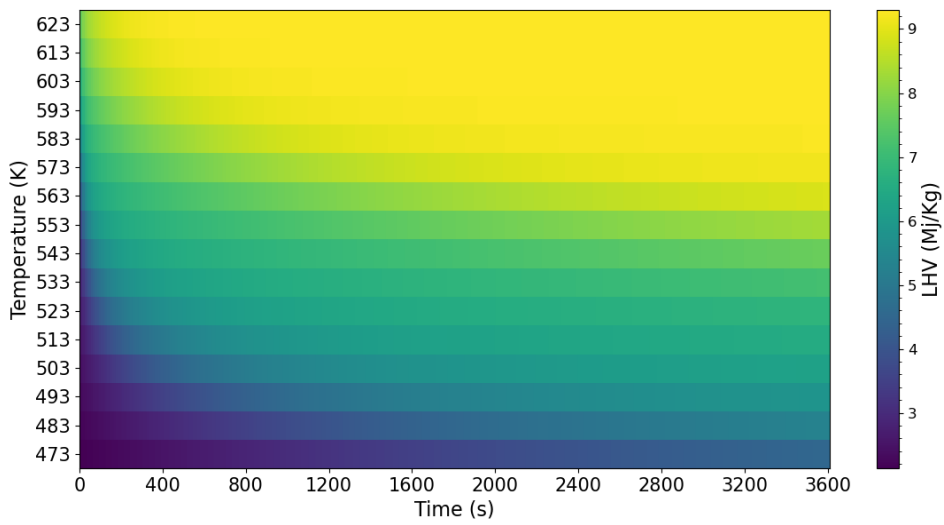
(a)



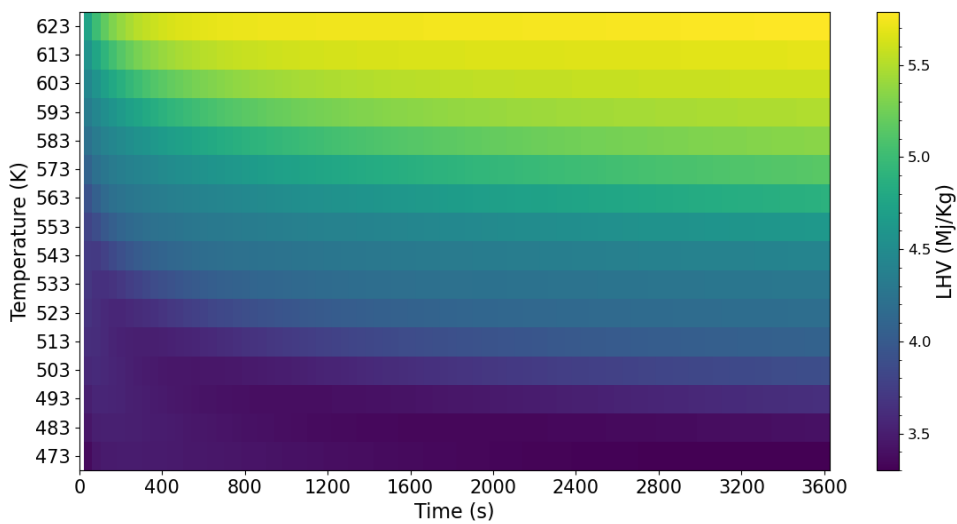
(b)

Figure 4.15: Energy densification as a function of the temperature and residence time for the adapted model (a) and pyrolysis (b).

From Figure 4.15 there is energy densification in both kinetic schemes. The evolution of this parameter is exactly the same as the LHV, since it is the current heating value in regards to the original heating value. The adapted model predicts higher energy densification, this might be due to the lower yields of liquid and gas on the adapted model, which means that there is less energy in the liquid and gas phases, therefore, the solid retains more energy, leading to a greater heating value of the torrefied biomass.



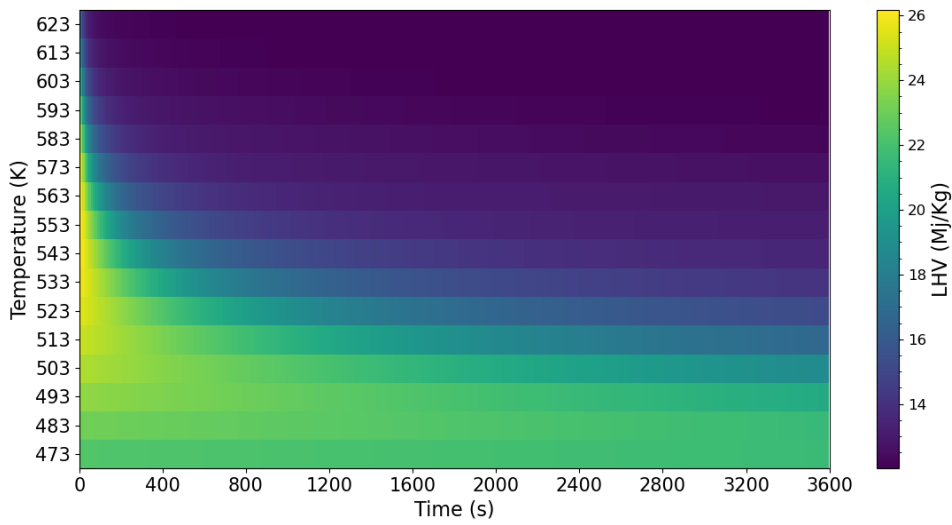
(a)



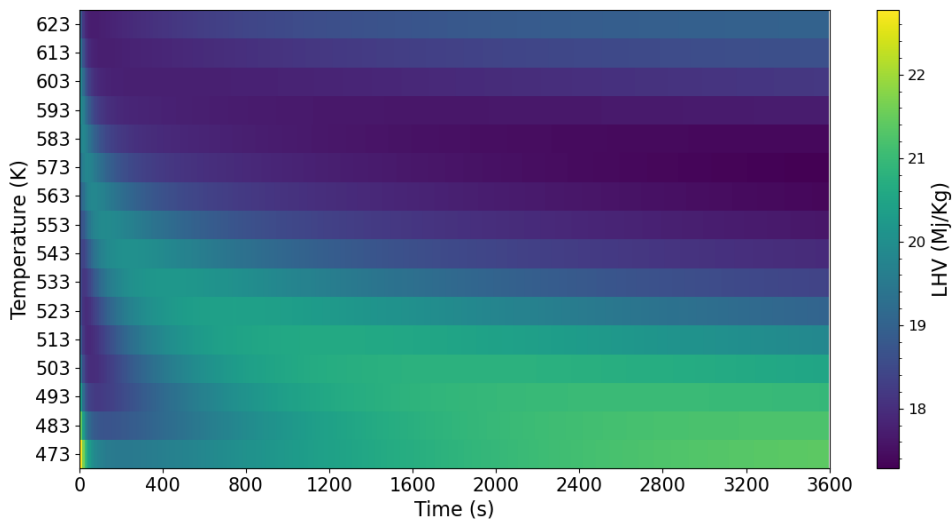
(b)

Figure 4.16: Gas LHV as a function of the temperature and residence time for the adapted model (a) and pyrolysis (b).

From Figure 4.16 the adapted model presents a higher heating value per kilogram of released gas, this is mainly due to the gas composition. Despite the over predicting of CO, which is the main contributor for the heating value of the released gases, the adapted model, released H₂, even though its presence is relatively small the LHV of H₂ is 11.8 times larger than the CO LHV. Similarly, the presence of CH₄, despite being small, can introduce some deviation, as its LHV is 4.9 times larger than the CO LHV. Therefore, the inaccuracy of the released gases might lead to the miss prediction of this parameter.



(a)



(b)

Figure 4.17: Liquid LHV as a function of the temperature and residence time for the adapted model (a) and pyrolysis (b).

From Figure 4.17 both kinetic schemes predict that the liquids with higher LHV are generated at lower temperatures, which goes into accordance with the results presented previously. Since that for higher temperatures there is more energy contained in the solid and gas phases, the liquid phase has a lower energy content.

Chapter 5

Conclusions

It was implemented a torrefaction kinetic scheme with several parameters that could vary accordingly to biomass composition and imposed temperature. Although the kinetic scheme from Anca-Couce et al. [18] was validated for woody biomass, there were several parameters that could be changed in order to accommodate the use of other biomass types. On an attempt to predict the behaviour of agricultural biomass, a tool was developed in order to account for the relevant points and its deviations. The best points were found and the one which provided the smallest error was further adapted to fit the experimental data. The adaptations consisted on a kinetic parameter adjustment, and the adjustment of specific molar coefficients. After the adjustments, the new kinetic scheme improved significantly on gas composition predictions, which was a major factor for the purpose of this work. Since the devolatilization profile is extremely important in this context, as torrefaction is used as a pre-treatment for gasification, therefore, it is out of interest to preserve the volatile matter to be later released during the thermochemical process. Despite the adapted model having a deviation over 30 %, out of all the previous kinetic schemes available, it provided the best predictions overall. The obtained results are only valid for the biomass in use and the imposed temperature profile. The proposed objectives were achieved successfully for the purpose of the given work.

5.1 Future Work

During the development of the present work, some aspects could not be explored, which are relevant to close the gap in kinetic modelling torrefaction of non-woody biomass. The major aspect that needs to be further explored is the molar coefficients of the released volatile matter, which might have to be optimised individually, instead of having several coefficients multiplied by the same factor (x_i). Overall, the model has to be restructured as the liquid and gas yields do not fit the experimental results. Gathering more experimental data from different non-woody biomass samples for a greater temperature range might be helpful to optimise the proportions at which the products are released.

Bibliography

- [1] Associação portuguesa de energias renováveis. <https://www.apren.pt/pt/energias-renovaveis/producao>. accessed: 20.08.2021.
- [2] S. Ferreira, E. Monteiro, P. Brito, and C. Vilarinho. Biomass resources in portugal: Current status and prospects. *Renewable and Sustainable Energy Reviews*, 78:1221–1235, October 2017. doi: 10.1016/j.rser.2017.03.140.
- [3] J. S. Tumuluru, S. Sokhansanj, J. R. Hess, C. T. Wright, , and R. D. Boardman. A review on biomass torrefaction process and product properties for energy applications. *Industrial Biotechnology*, 7(5), October 2011. doi:10.1089/ind .2011.0014.
- [4] M. Strandberg, I. Olofsson, L. P. SusanneWiklund-Lindströma, K. Åberg, and A. Nordin. Effects of temperature and residence time on continuous torrefaction of spruce wood. *Fuel Processing Technology*, 134:387–398, June 2015. doi:10.1016/j.fuproc.2015.02.021.
- [5] K.-M. Lu, W.-J. Lee, W.-H. Chen, S.-H. Liu, and T.-C. Lin. Torrefaction and low temperature carbonization of oil palm fiber and eucalyptus in nitrogen and air atmospheres. *Bioresource Technology*, 123:98–105, November 2012. doi:10.1016/j.biortech.2012.07.096.
- [6] P. C. Bergman and J. H. Kiel. Torrefaction for biomass upgrading. *14th European Biomass Conference and Exhibition, Paris, France*, pages 17–21, October 2005.
- [7] M. G. Martínez, P. Floquet, C. Dupont, D. da Silva Perez, and X. mi Meyer. Assessing the impact of woody and agricultural biomass variability on its behaviour in torrefaction through principal component analysis. *Biomass abd Bioenergy*, 134, March 2020. doi:10.1016/j.biombioe.2020.105474.
- [8] P. Basu. *Biomass Gasification, Pyrolysis, and Torrefaction Practical Design and Theory*, chapter 4. Elsevier Inc., second edition, 2013.
- [9] W.-H. Chenand and P.-C. Kuor. A study on torrefaction of various biomass materials and its impact on lignocellulosic structure simulated by a thermogravimetry. *Energy*, 35(6):2580–2586, June 2010. doi:10.1016/j.energy.2010.02.054.
- [10] J. Wannapeera, B. Fungtammasan, and N. Worasuwannarak. Effects of temperature and holding time during torrefaction on the pyrolysis behaviors of woody biomass. *Journal of Analytical and Applied Pyrolysis*, 92(1):99–105, September 2011. doi:10.1016/j.jaap.2011.04.010.

- [11] A. Pimchuai, A. Dutta, and P. Basu. Torrefaction of agriculture residue to enhance combustible properties. *Energy Fuels*, 24(9):4638–4645, February 2010. doi:10.1021/ef901168f.
- [12] V. Repellin, A. Govin, M. Rolland, and R. Guyonnet. Energy requirement for fine grinding of torrefied wood. *Biomass and Bioenergy*, 34(7):923–930, July 2010. doi: 10.1016/j.biombioe.2010.01.039.
- [13] P. Basu. *Biomass Gasification, Pyrolysis, and Torrefaction Practical Design and Theory*, chapter 3, pages 54–60, 80. Elsevier Inc., second edition, 2013.
- [14] K. S. Kunga, S. K. Thenganea, and A. F. Ghoniema. Functional mapping of torrefied product characteristics with index of torrefaction. *Fuel Processing Technology*, 202(106362), June 2020. doi: 10.1016/j.fuproc.2020.106362.
- [15] A. Sarvaramini, G. P. Assima, and F. Larachi. Dry torrefaction of biomass – torrefied products and torrefaction kinetics using the distributed activation energy model. *Chemical Engineering Journal*, 229:498–507, August 2013. doi: 10.1016/j.cej.2013.06.056.
- [16] R. Mehrabian, A. Anca-Couce, R. Scharler, I. Obernberger, W. Janisch, and K. Trattner. Release of gaseous compounds during torrefaction: results from test runs and modelling. *21st European Biomass Conference and Exhibition*, June 2013.
- [17] E. Ranzi, A. Cuoci, T. Faravelli, A. Frassoldati, G. Migliavacca, S. Pierucci, and S. Sommariva. Chemical kinetics of biomass pyrolysis. *Energy Fuels*, 22(6):4292–4300, January 2009. doi: 10.1021/ef800551t.
- [18] A. Anca-Couce and I. Obernberger. Application of a detailed biomass pyrolysis kinetic scheme to hardwood and softwood torrefaction. *Fuel*, 167:158–167, March 2016. doi: 10.1016/j.fuel.2015.11.062.
- [19] P. Debiagi, G. Gentile, A. Cuoci, A. Frassoldati, E. Ranzi, and T. Faravelli. A predictive model of biochar formation and characterization. *Journal of Analytical and Applied Pyrolysis*, 134:326–335, September 2018. doi: 10.1016/j.jaap.2018.06.022.
- [20] S. V. Vassilev, D. Baxter, L. K. Andersen, C. G. Vassileva, and T. J. Morgan. An overview of the organic and inorganic phase composition of biomass. *Fuel*, 94:1–33, April 2012. doi:10.1016/j.fuel.2011.09.030.
- [21] C. Tezara, J. Siregar, H. Lim, F. Fauzi, M. Yazdi, L. Moey, and J. Lim. Factors that affect the mechanical properties of kenaf fiber reinforced polymer: A review. *Journal of Mechanical Engineering and Sciences*, 10(2):2159–2175, September 2016. doi: 10.15282/jmes.10.2.2016.19.0203.
- [22] D. X. Zhou, D. W. Li, D. R. Mabon, and P. L. J. Broadbelt. A critical review on hemicellulose pyrolysis. *Energy Technology*, 5(1):52–79, January 2017. doi: 10.1002/ente.201600327.
- [23] L. R. S. Moreira and E. X. F. Filho. An overview of mannan structure and mannan-degrading enzyme systems. *Applied Microbiology and Biotechnology volume*, (79):165–178, 2008. doi: 10.1007/s00253-008-1423-4.

- [24] P. Parthasarathy, K. S. Narayanan, and L. Arockiam. Study on kinetic parameters of different biomass samples using thermo-gravimetric analysis. *Biomass and Bioenergy*, 58:58–66, November 2013. doi: 10.1016/j.biombioe.2013.08.004.
- [25] M. R. B. Guerrero, M. M. da Silva Paula, M. M. Zaragoza, J. S. Gutiérrez, V. G. Velderrain, a. L. Ortiz, and V. Collins-Martínez. Thermogravimetric study on the pyrolysis kinetics of apple pomace as waste biomass. *International Journal of Hydrogen Energy*, pages 1–9, 2014.
- [26] A. Hornung, F. Stenzel, and J. Grunwald. Biochar—just a black matter is not enough. *Biomass Conversion and Biorefinery*, January 2021. doi: 10.15282/jmes.10.2.2016.19.0203.
- [27] A. Demirbas and G. Arin. An overview of biomass pyrolysis. *Energy Sources*, 24(5):471–482, 2002. doi:10.1080/00908310252889979.
- [28] Biomass carbonization. <https://www.intechopen.com/books/renewable-energy-resources-challenges-and-applications/biomass-carbonization>. accessed: 10.2021.
- [29] Python. <https://www.python.org/>. accessed: 03.2021.
- [30] Cantera. <https://cantera.org/>. accessed: 03.2021.
- [31] A. Ferreira, R. Segurado, and M. Costa. Modelling soot formation during biomass gasification. *Renewable and Sustainable Energy Reviews*, 134(110380), December 2020. doi: 10.1016/j.rser.2020.110380.
- [32] D. R. Nhuchhen and M. T. Afzal. Hhv predicting correlations for torrefied biomass using proximate and ultimate analyses. *Bioengineering*, 4, January 2017. doi: 10.3390/bioengineering4010007.
- [33] M. J. Moran, H. N. Shapiro, D. D. Boettner, and M. B. Bailey. *Fundamentals of engineering thermodynamics*, chapter 13. John Wiley Sons, Inc., seventh edition, 2011.
- [34] E. Ranzi, P. E. A. Debiagi, and A. Frassoldati. Mathematical modeling of fast biomass pyrolysis and bio-oil formation. note i: Kinetic mechanism of biomass pyrolysis. *ACS Sustainable Chem. Eng.*, 5(4):2867–2881, 2017. doi: 10.1021/acssuschemeng.6b03096.
- [35] R. A. Patil. Cleavage of acetyl groups for acetic acid production in kraft pulp mills. Master's thesis, The University of Maine, 2012.
- [36] I. Spiridon and V. I.Popa. Chapter 13 - hemicelluloses: Major sources, properties and applications. *Monomers, Polymers and Composites from Renewable Resources*, pages 289–304, 2008. doi: 10.1016/B978-0-08-045316-3.00013-2.
- [37] K. Dussan, S. Dooley, and R. Monaghan. Integrating compositional features in model compounds for a kinetic mechanism of hemicellulose pyrolysis. *Chemical Engineering Journal*, 328:943–961, November 2017. doi: 10.1016/j.cej.2017.07.089.

- [38] P. Debiagi, C. Pecchi, G. Gentile, A. Frassoldati, A. Cuoci, T. Faravelli, and E. Ranzi. Extractives extend the applicability of multistep kinetic scheme of biomass pyrolysis. *Energy Fuels*, 29: 6544–6555, 2015. doi: 10.1021/acs.energyfuels.5b01753.